REVIEW ARTICLE
PUBLISHED ONLINE: 7 NOVEMBER 2017 | DOI: 10.1038/NNANO.2017.218

nature nanotechnology

High-performance semiconductor quantum-dot single-photon sources

Pascale Senellart[1]*, Glenn Solomon[2] and Andrew White[3]

Single photons are a fundamental element of most quantum optical technologies. The ideal single-photon source is an on-demand, deterministic, single-photon source delivering light pulses in a well-defined polarization and spatiotemporal mode, and containing exactly one photon. In addition, for many applications, there is a quantum advantage if the single photons are indistinguishable in all their degrees of freedom. Single-photon sources based on parametric down-conversion are currently used, and while excellent in many ways, scaling to large quantum optical systems remains challenging. In 2000, semiconductor quantum dots were shown to emit single photons, opening a path towards integrated single-photon sources. Here, we review the progress achieved in the past few years, and discuss remaining challenges. The latest quantum dot-based single-photon sources are edging closer to the ideal single-photon source, and have opened new possibilities for quantum technologies.

In the past century, technology was transformed by the first quantum revolution, where utilization of some aspects of quantum mechanics—such as energy quantization or wave–particle duality—enabled technologies ranging from semiconductor devices to lasers. We are at the threshold of a second quantum revolution, where new technologies will make use of previously untapped features of quantum mechanics, such as superposition, entanglement and quantum measurement[1]. Photonics—the generation, processing and detection of light—is a product of the first quantum revolution and, despite its name, until now has not exploited any features associated with photons, the individual particles of light.

Quantum photonics requires quantum light fields such as squeezed light[2], single photons or entangled photons. It promises to enable significant capabilities in: communication, for example, quantum key distribution[3] and tamper-proof voting protocols[4]; metrology and imaging, yielding devices with resolution and precision better than allowed by the quantum noise limit[5,6]; and quantum simulation and computation[7,8]. In the applications that require entanglement, such as quantum computation[9,10], a linear increase in hardware resources has the same effect as an exponential increase in conventional approaches[11].

For quantum photonics to realize its potential, three technologies are necessary: efficient, fast, photon counters[12], linear and nonlinear photonic circuits[13,14], and single-photon sources. While recent years have seen significant progress in photonic detection and linear circuits, a significant roadblock to further progress has been the lack of scalable photon sources.

The ideal single-photon source

Three properties are important to describe an ideal single-photon source. Depending on the scientific community, these three properties have been given different names but the important features behind them remain the same: a single-photon source should produce light pulses with no more than one photon, in a pure quantum state and as efficiently as possible.

Single-photon purity. A light pulse can be decomposed as an ensemble of plane wave modes, where each mode is a quantized harmonic oscillator with defined polarization $\boldsymbol{\varepsilon}$, spatial frequency $\mathbf{k}$, and frequency $\omega = ck$, where c is the speed of light. The photon wavepacket is

$$|\psi\rangle = \sum_{\mathbf{k},\boldsymbol{\varepsilon},n} c_{\mathbf{k},\boldsymbol{\varepsilon}} \; |n\rangle_{\mathbf{k},\boldsymbol{\varepsilon}}$$

The number state of each mode—or Fock state—written as $|n\rangle_{\mathbf{k},\boldsymbol{\varepsilon}}$, corresponds to a pure state with exactly n photons in the mode. A single-photon light field is built exclusively on single-photon Fock states $|1\rangle_{\mathbf{k},\boldsymbol{\varepsilon}}$, with a total photon number of one[15]. The fact that the field does not contain more than one photon can be characterized by the second-order intensity correlation function $g^{(2)}(0)$ measured using a Hanbury Brown and Twiss experiment (Box 1). A light field with no more than one photon leads to $g^{(2)}(0) = 0$ whereas a laser field gives $g^{(2)}(0) = 1$. $g^{(2)}(0)$ is often used to characterize the single-photon purity of the source. A high single-photon purity guarantees the security of quantum communications[16] and minimizes errors in quantum computation and simulation[17–20].

Indistinguishability. For many applications, the photons must be indistinguishable. Quantum technologies require effective photon–photon interactions to implement two-photon quantum gates, where the state of one photon is determined by the state of a second one. Such entangling gates are key elements in quantum algorithms or in quantum repeaters for long-distance quantum communication. The effective two-photon interaction can be engineered using the quantum interference of two single-photon wavepackets that cannot be distinguished from one another by any measurement (Box 1). This condition is reached when each wavepacket is a pure quantum state, with defined complex coefficients $c_{\mathbf{k},\boldsymbol{\varepsilon},n}$, not a statistical mixture. The indistinguishability is characterized by the mean photon wavepacket overlap M, which

[1]Center for Nanosciences and Nanotechnology CNRS, UMR9001, University Paris-Saclay, C2N – Site de Marcoussis, Route de Nozay, 91460 Marcoussis, France. [2]Joint Quantum Institute, National Institute of Standards and Technology, and University of Maryland, Gaithersburg, Maryland 20889, USA. [3]Centre for Engineered Quantum Systems and Centre for Quantum Computer and Communication Technology, School of Mathematics and Physics, University of Queensland, Brisbane, Queensland 4072, Australia. *e-mail: pascale.senellart-mardon@c2n.upsaclay.fr

Box 1 | Characterizing a single-photon source.

Measuring the single-photon purity. A simple way to test whether a light field has no more than one photon is to perform the Hanbury Brown and Twiss experiment[189]. The case of pulsed light—that is, on-demand sources—is discussed here. The light field is sent to a beamsplitter and two single-photon detectors D_1 and D_2 measure each output (panel a). The detector outputs are sent to correlation electronics that measure the time delay between coincident detection events, that is, events where both detectors fire. An example of such detection coincidences is presented in Fig. 1f as a function of time delay. Correlations are observed at multiples of the source repetition time, corresponding to coincidences for photons emitted in different pulses. The area of the peak at zero delay—where a coincidence only arises if more than one photon was present in the light pulse—provides information on the single-photon purity. In detail, the second-order correlation function is

$$g^{(2)}(0) = \frac{\langle n_1(t) n_2(t)\rangle_t}{\langle n_1(t)\rangle_t \langle n_2(t)\rangle_t}$$

where $n_i(t)$ is the number of counts (n) detected on D_i at time t. So measuring $g^{(2)}(0)$ then gives access to the single-photon purity: if $p(n)$ is the n-photon number probability[190], $g^{(2)}(0) \approx 2p(2)/p(1)^2$ for $p(1) >> p(2) >> p(n > 2)$. For an ideal single-photon source, $p(2) = 0$ and $g^{(2)}(0) = 0$. Note that this experiment, based on detection events, does not give access to the vacuum component of the field $p(0)$: this characteristic of the source is discussed in the brightness section of the main text.

Measuring the photon indistinguishability. The mean wavepacket overlap of two light wavepackets can be measured through the Hong–Ou–Mandel experiment[21]. When two indistinguishable photon wavepackets, described by the same pure quantum state, are sent to the two inputs of a beamsplitter with perfect spatial and temporal overlap, a quantum interference process takes place. The probability amplitudes of the events 'both photons transmitted' and 'both photons reflected' interfere destructively due to the relations between the reflection and transmission coefficients of the beamsplitter. As a result, both light wavepackets scatter into the same output. This bunching or coalescence can be measured by the visibility of the quantum interference V_{HOM} and is directly linked to the photon wavepacket overlap M. The second-order coincidence count $C_{||}$ is measured between two detectors located on two outputs (panel b). For normalization, the light pulse in one input arm can be made maximally distinguishable by varying a degree of freedom—commonly the pulse arrival time at the beamsplitter or polarization, cancelling the quantum interference effect, yielding a coincidence count $C_{\perp}$. The HOM visibility is $V_{HOM} = (C_{\perp} - C_{||})/C_{\perp}$. The coincidence counts are integrated over the entire pulse temporal duration, as any temporal post-selection artificially increases V_{HOM}. The indistinguishability is given by $M = V_{HOM}((R^2 + T^2)/2RT)$ where $T = 1 - R$ and R and T are the beamsplitter intensity reflectivity and transmission coefficients, respectively, and when $R = T = 0.5$, the V_{HOM} visibility is simply the indistinguishability M.

Sources with imperfect single-photon purity, $g^{(2)}>0$, yield $V_{HOM} < 1$ since the additional photon terms give coincidences in both $C_{||}$ and $C_{\perp}$. In QD single-photon sources, the indistinguishability and single-photon purity can be independently controlled. It is therefore common to extract an indistinguishability M^* corrected from the imperfect single-photon purity when $g^{(2)}(0) << 1$: it characterizes the wavepacket overlap for all degrees of freedom other than photon number and is given by $M^* = M + g^{(2)}(0)$. Making such a distinction allows a more precise diagnosis of what limits performance when developing single-photon sources. Note that for quantum optics experiments and applications, the indistinguishability M remains the relevant figure of merit, which requires both highly indistinguishable photons and high single-photon purity.

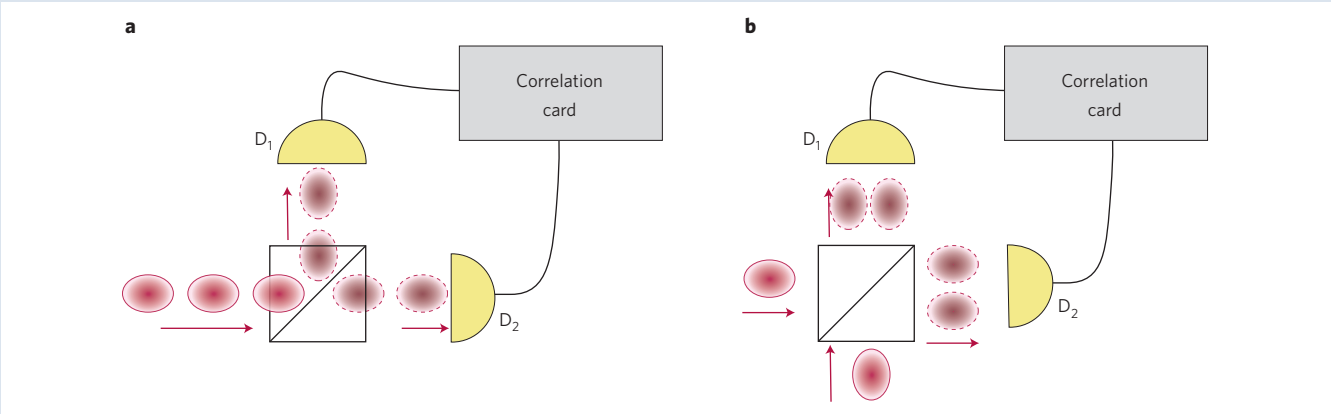

can be measured through Hong–Ou–Mandel (HOM) interference[21]: the two light pulses are sent to the two inputs of a beamsplitter, with one detector at each output. If the two light pulses are in the same pure quantum state, they exit the beamsplitter together, and only one detector senses the photons. The HOM visibility V_{HOM} of the quantum interference is determined through the second-order correlations between the detectors, yielding the indistinguishability M (Box 1). Perfect indistinguishability is characterized by $M = 1$.

Brightness. Finally, a deterministic single-photon source should deliver light pulses with no vacuum component, |0>. This property is very fragile as any optical loss leads to a vacuum component. How close a source is to deterministic operation thus depends on where the single photon probability is measured: at the output of the source, at the output of an optical fibre, on a detector, and so on. As a result, the efficiency or brightness of a single-photon source has not been defined in a uniform way among various communities. Many figures of merit are used, including count rates on a detector, collected photons per second and brightness at the first lens. The appropriate choice depends on perspective, and comparisons can be challenging.

A good measure is the probability B that each light pulse contains a single photon: $B = 1$ for a deterministic single-photon source.

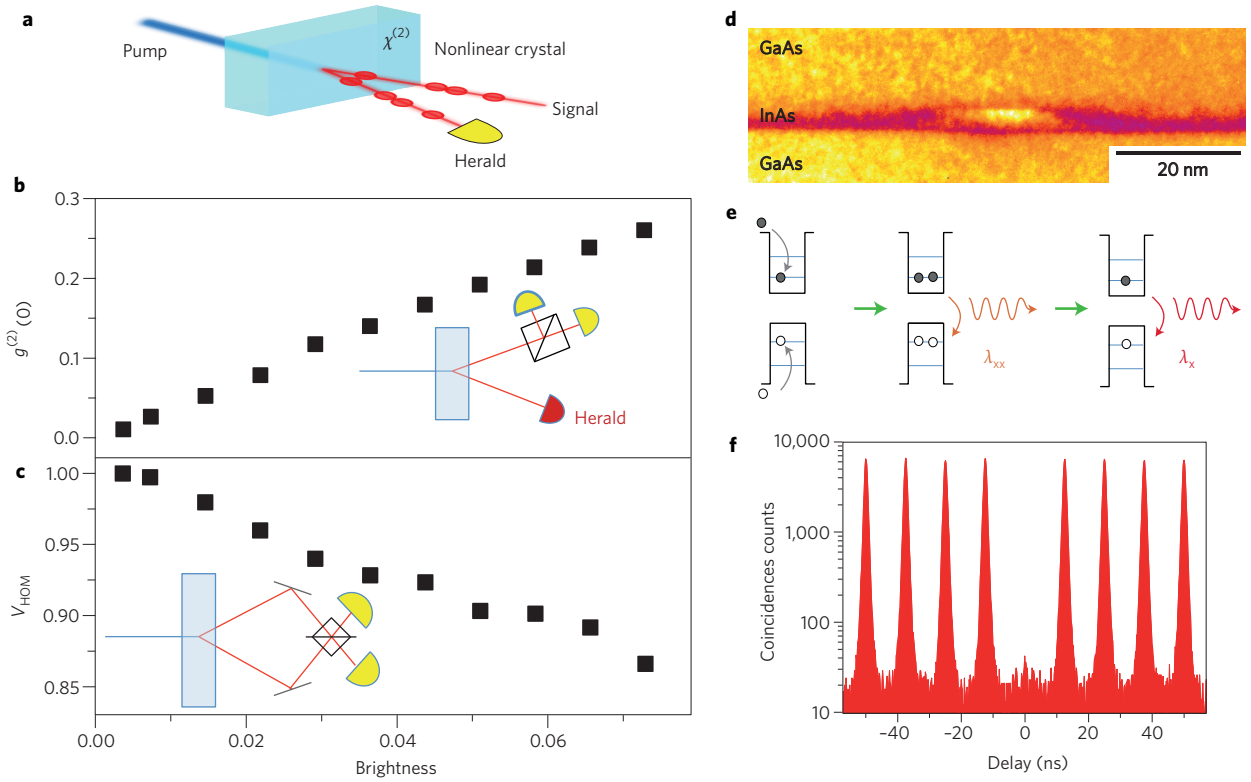

Figure 1 | Spontaneous parametric down-conversion (SPDC) and QD-based single-photon sources. a, Schematic of a SPDC source: a pulsed laser is sent to interact with a nonlinear crystal. The crystal temperature and angle are adjusted to obtain the phase-matching condition. Photon pairs are generated: one, the idler, can be used to herald the other, the signal. **b**, Measured $g^{(2)}(0)$ for a SPDC source as a function of brightness. The inset shows the measurement scheme: the correlation measurement on the signal is conditioned on the detection of a heralding event on the idler. **c**, Measured V_{HOM} for a SPDC source as a function of brightness. The inset shows the measurement scheme: pairs of photons from the same down-conversion pairs are sent on the beamsplitter. **d**, Transmission electron microscopy of a single self-assembled InGaAs quantum dot. **e**, Schematic of the radiative cascade of carriers in a QD: electrons and holes created in the barrier relax in the QD through carrier collisions or interaction with phonons (grey arrows). Once in the QD, the carriers radiatively recombine by successively emitting photons in a cascade. The last two emitted photons in a neutral exciton cascade are emitted at different wavelengths (λ_{XX}, λ_X) because of Coulomb interaction. A single photon is emitted at each wavelength. **f**, Example of a Hanbury Brown and Twiss measurement (coincidence counts) obtained under pulsed excitation on the bright single-photon source reported in ref. 118. The data are plotted on a logarithmic scale and show, when normalized, that $g^{(2)}(0) = 0.0056 \pm 0.0011$. Panels adapted from: **b**,**c**, ref. 33, Macmillan Publishers Ltd; **f**, ref. 118, OSA.

If $p(n)$ is the n-photon number probability (see Box 1), then $B = p(1)$ for $p(1) >> p(n > 1)$. We use this metric here as it allows comparison of systems independent of the pulsed-operation rate or detector efficiency. Together with the source repetition rate, the transmission of the optical network and detector efficiencies, B determines the speed of quantum communications or computation protocols. For many practical implementations, an important figure is the brightness measured at the output of a single mode fibre, B_{SMF}.

The lower the brightness of a single-photon source, the poorer the system scaling. For instance, in the generation of n-manifold single photons, the probability scales with brightness to the power n. The lack of scalable single-photon sources has become one of the major roadblocks in the development of quantum photonics. This can be clearly seen in the measured photon production rates in the literature, which drop seven orders of magnitude between megahertz rates[22] for $n = 1$, to 0.1 Hz rates[23] for $n = 5$, motivating many groups to fabricate inherently deterministic—and hence scalable—single-photon sources.

Finally, depending on the application, various modal properties are desired. Some applications, such as quantum key distribution, can use a single source emitting single photons into orthogonal temporal modes within the same spatial mode. Others, such as quantum metrology, require a manifold single-photon source, with n orthogonal spatial modes, each containing a single photon within the same temporal mode. The latter can be achieved by either using multiple single-photon sources or by demultiplexing a single source.

Single-photon sources

The most common single-photon sources are based on nonlinear frequency conversion or on the spontaneous emission of single quantum emitters.

Spontaneous parametric down-conversion source. To date, the best-performing and most widely used sources have been based on nonlinear frequency conversion[24]. As such, they represent the benchmark for any new single-photon source technology. They are robust and operate at, or near, room temperature using frequency conversion, specifically down-conversion in a $\chi^{(2)}$ media such as nonlinear crystals[25,26] (Fig. 1a), or a $\chi^{(3)}$ media such as glass, dilute atomic gases or silicon[27,28]. Here, $\chi^{(2)}$ and $\chi^{(3)}$ are the 2nd and 3rd order susceptibilities of the medium, respectively. Pairs of down-converted photons are produced at a linear rate in the pump field intensity—a process known as spontaneous parametric down-conversion (SPDC). The process is non-deterministic: photon pairs are generated at random times. However, the conditions can be set so that the photons in the two down-converted modes are non-degenerate—in frequency, polarization or spatial mode—ensuring that they can be subsequently split deterministically. In such cases, the photons in

one mode are sent to a detector, and a detection event heralds with high probability the presence of the twin photon in the other mode. With appropriate frequency and spatial filtering, SPDC sources have been shown to provide pure, highly indistinguishable, single photons, and can also produce polarization-entangled photon pairs[29]. Down-conversion efficiency has been constantly improved[30]—by seven orders of magnitude in just over a decade—and implementations have moved from bulk[25,26] to integrated optics[31].

A critical issue in down-conversion is the fact that the probability of creating n pairs scales with pump intensity to the nth power. Although the heralding process removes the zero photon-pair component of the field, it does not alter the probability of generating more than one pair. Increasing the power thus greatly increases the probability of heralding an event that has multiple photons, leading to increased $g^{(2)}(0)$ with pump intensity, and decreased utility in applications[32]. Figure 1b,c shows the single-photon purity and HOM visibility measured on a heralded SPDC source as a function of brightness, defined here as the generation probability for a single pair. The $g^{(2)}(0)$ rapidly deteriorates with the brightness, reaching 0.2 for a source that contains only one pair every 20 pulses. Similarly, Fig. 1c presents the HOM visibility measured when sending the two photons from the same pair-generation event on a beamsplitter. Close to unity visibility can be observed, but this decreases significantly with brightness because of multi-pair events[34].

Unless it is specifically engineered away, the photons from down-conversion are frequency entangled. This does not affect the HOM visibility between photons from the same pair. However, it significantly reduces the visibility between photons from successively generated photon pairs[32], hence degrading the utility of the photons in applications[35]. Recent years have seen substantial progress in engineering frequency-uncorrelated SPDC sources[36,37]. This is a necessary step in multiplexing sources[38] to increase overall source efficiency, an idea first proposed in 2002. Multiplexing was demonstrated in 2016: with four photons, achieving a two-fold increase in single-photon output probability without introducing additional multi-photon noise, but yielding 69±3.4% HOM visibility in the multiplexed photons[39]; and with eight photons, achieving 1.5–1.8-fold brightness increases over the mean of the non-multiplexed sources, but with no indistinguishability measurements of the multiplexed photons[40].

Single-emitter based sources. The spontaneous emission from a two-level system is inherently single-photon like. Early demonstrations of single-photon emission were based on atoms[41], ions[42] and molecules[43], and followed by demonstrations with artificial atoms in a solid-state environment. Unlike attenuated lasers or SPDC sources, the brightness of these sources can be intrinsically decoupled from the single-photon purity.

Solid-state systems offer a diverse catalogue of single-photon sources. Scalability and integration are obvious advantages, while decoherence due to coupling to the solid-state environment is often an issue. Epitaxial semiconductor quantum dots (QDs) have been widely investigated in the past decade, with a large variety of materials, such as InGaAs for near infrared emission[44], GaAs for emission in the red spectral range[45], and II–VI telluride or selenide based QDs[46,47], as well as nitride based III–V QDs[48], for emission in the green to ultraviolet spectral range. Depending on the bandgap, single-photon emission is achieved at temperatures ranging from cryogenic to room temperature. Colloidal QDs offer bright, room-temperature single-photon emission[49], recently with reduced blinking phenomena[50]. The nitrogen-vacancy centre, a complex defect in diamond with a stable spin-triplet ground-state, generates single photons; however, it is hampered by phonon coupling and only a small fraction of the light is emitted in the zero-phonon line even at cryogenic temperatures. This fraction can be strongly increased by coupling nitrogen vacancies to microcavities[51–53]. Other single-photon emitters have recently emerged, such as the silicon-vacancy complex in diamond, rare-earth atomic dopants[54] and defects in two-dimensional monolayer materials[55–58]. For an overview of these solid-state photon emitters, we refer to a recent review paper[59]. Here, we focus on the substantial progress made by the epitaxial QD community—mostly using InGaAs-based QDs—for which the single-photon sources have recently reached very high performance levels. For the first time, these sources outperform the long-used SPDC sources, and open new perspectives for quantum optical technologies.

Basics of QD-based single-photon sources

At present, the best-performing QD-based single-photon sources are made using III–V semiconductors. III–V QDs have large optical dipoles, resulting in a large coupling with confined or guided optical modes, a key feature in obtaining bright sources. We review the physics at play in III–V QDs, as well as the highly mature technologies that have been developed to fabricate state-of-the-art single-photon sources. Similar physics and technological approaches can benefit the development of single-photon sources using other quantum emitters and materials.

QD growth. Self-assembled epitaxial QD growth is briefly described here for InAs-based QDs in GaAs. InAs and GaAs are covalently bonded direct-bandgap semiconductors, where the bandgap energies are E_g(InAs) = 0.43 eV and E_g(GaAs) = 1.52 eV at 4 K. The 7% lattice-constant mismatch between GaAs and InAs precludes the typical epitaxial planar-crystal growth process. When more than 1.7 monolayers of InAs is deposited on GaAs, a planar layer forms—called the wetting layer—that is biaxially compressed to the GaAs lattice. As crystal growth proceeds, the accumulated strain energy increases, a transition occurs and the total energy is minimized by creating InAs islands[60–62]. By stopping the growth right after this transition, the islands are typically 10–30 nm lateral size in the in-plane directions and 2–5 nm out of plane[63–65] (Fig. 1d). When further covered with epitaxial GaAs, three-dimensional quantum confinement shifts the lowest optical transitions in the 900–1,000 nm wavelength range at 4 K (refs 66,67). The transitions can be brought to 1.3 μm for large QDs covered in InGaAs. InGaAs QDs naturally have a slight asymmetry in their in-plane shape. Other QD growth techniques, such as droplet epitaxy[68], can be used to obtain higher symmetry QDs[69].

Randomness. As strain-driven and droplet QDs are naturally formed, they have random spatial positions. Light emission from an ensemble is inhomogeneously broadened because of QD size fluctuations and local environmental variations, but the QDs have close to unity quantum efficiency and low dephasing when they are far from processed interfaces. Ordering of QDs by crystal growth on lithographic patterned samples has been extensively investigated[70–72] with continuous improvements, but the proximity to previously processed surfaces still diminishes the quantum efficiency and coherence of emitted photons. Reduction of the QD inhomogeneous distribution is desired for the development of identical single-photon sources. Growing two QDs of exactly the same energy within the radiative linewidth remains out of reach—considering the QD nanometre scale, especially in the vertical direction—with the lowest inhomogeneous broadening being still in the nanometre range[73]. Yet, this inhomogeneous broadening can be overcome by applying strain or electrical fields that can tune individual states to a common frequency[74–77].

Energy levels. The strong quantum confinement in QDs leads to discrete energy levels for both electrons and holes. Carrier localization and Coulomb and exchange interactions lead to excitonic many-body states. Pauli exclusion leads to a ground-state manifold

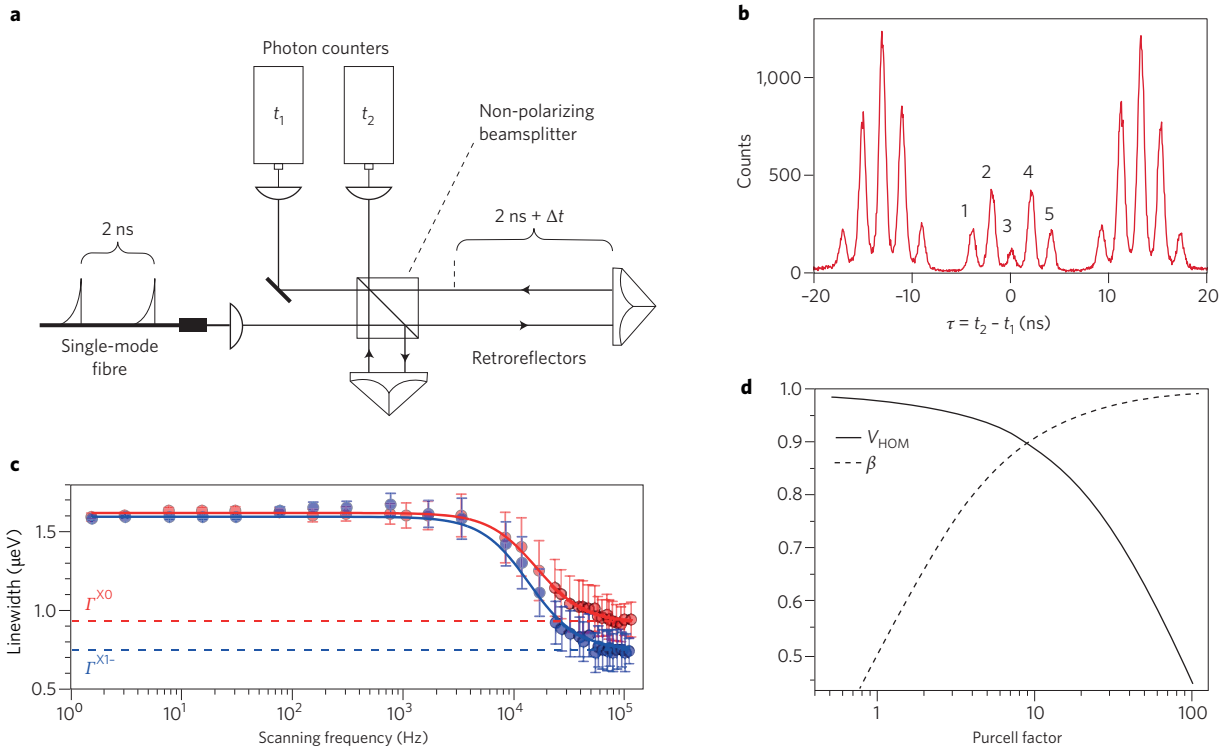

Figure 2 | Indistinguishability of QD-based single-photon sources. a, Schematic of one type of HOM measurement performed on a single-photon source: two photons emitted by the same QD with a 2 ns delay are sent to a Mach–Zehnder interferometer with a 2 ns delay in one arm. **b**, First demonstration of indistinguishable photons from a QD[100]. The figure shows the histogram of coincidences at the output of the setup presented in **a**. Five peaks are observed for repetition rate of the laser due to the different possible paths followed by the first and second photons. The strongly reduced area of the peak at zero delay demonstrates an indistinguishability of around 80%. **c**, Linewidth of an exciton (red) and charged exciton (blue) line for varying acquisition times. The radiative limited linewidth is indicated by the dotted horizontal line, showing the negligible effect of charge and spin noise for timescales below 10 μs. **d**, Calculated HOM visibility V_{HOM} and coupling to a cavity mode β as a function of the Purcell factor showing the compromise between high efficiency and high indistinguishability for a non-resonant QD excitation. Panels **a** and **b** reproduced from ref. 100, Macmillan Publishers Ltd. Panels adapted from: **c**, ref. 117, Macmillan Publishers Ltd; **d**, ref. 99, APS.

consisting of: two optically bright excitons |X⟩—one electron and one hole with projection of the total angular momentum along the growth axis $J_z = \pm 1$; two lower-energy dark excitons, $J_z = \pm 2$; a single bright biexciton, |XX⟩—two electrons and two holes; and two charged excitons known as trions—single excitons containing either an excess electron $|X^-\rangle$ or hole $|X^+\rangle$. Anisotropic exchange results in a mixing of the $J_z = \pm 1$ states, leading to two split, linearly polarized neutral-excitonic optical transitions, while the circular polarization remains for the charged ones.

Radiative cascade. Under non-resonant excitation to either the GaAs bulk or the wetting layer, carriers rapidly diffuse to the QD states through carrier collisions and optical phonon emission. Under strong excitation, the QD is filled with carriers and a radiative cascade takes place: a single photon is emitted during the decay from the |XX⟩ state to either of two bright |X⟩ states, and another photon is emitted from the |X⟩ to the QD ground state[78,79] (Fig. 1e). Because of the strong Coulomb interaction between carriers, the wavelength of the optical transition of |XX⟩ → |X⟩ differs from that of |X⟩ → |0⟩ by typically a few nanometres. Spectral filtering of a single emission line is used to obtain a single-photon source. Non-resonant excitation is experimentally convenient as the excitation laser is easy to separate from the single-photon emission. However, as discussed below, it limits source performances in terms of indistinguishability. While more challenging, direct resonant excitation of the |X⟩ state[80,81], as well as resonant excitation of the |XX⟩ state through a two-photon absorption process[82], have been demonstrated and are now used to obtain high indistinguishability[83,84].

Single-photon emission. The emission from a single epitaxial QD was isolated in 1994[66,67] and single-photon emission was demonstrated in 2000 through second-order photon correlation $g^{(2)}(0)$ measurements[44] (Box 1). First demonstrations were done under optical pumping, followed later by electrical pumping[85]. Obtaining low $g^{(2)}(0)$ under non-resonant pulsed excitation requires that for a given pulse, no carriers are captured and recombine in the QD after a first exciton emission. This requires that relaxation into the QD and the radiative cascade leading to the exciton recombination occur on a longer timescale than the decay time of the population of initially created carriers[86,87]. Low values of $g^{(2)}(0)$ can be more systematically obtained using direct excitation into an excited state of the QD. Under strictly resonant excitation, such considerations no longer apply and values of $g^{(2)}(0)$ below 1% have been reported[33,83,88–90].

Single entangled photon-pair generation. QDs can also generate polarization-entangled photon-pairs: the radiative decay of |XX⟩ occurs through two paths to either of the two bright |X⟩ states, after which the |X⟩ states radiatively decay to the ground state[78,79]. In an ideal QD, the two |X⟩ states are energy degenerate and the bifurcated cascade provides no which-path information, so that a polarization-entangled two-photon state is emitted[69,91–93]. However, anisotropic exchange usually leads to |X⟩ energy splitting, restoring which-path information and diminishing entanglement. This energy splitting can be minimized by precisely controlling the QD shape during the growth[94]. Moreover, various fields—electrical[74], magnetic[95], strain[96] and optical[97]—applied to

the QD can cancel this splitting and Bell inequality violations are routinely reported[96,98].

Indistinguishability

The ability to generate a pure quantum state of light is measured by performing a HOM measurement (see Box 1): single-photon wavepackets successively generated by the same emitter with a time delay of Δt are temporally overlapped on a beamsplitter. Since the emitter is point like, the spatial coherence is decoupled from the temporal one: one can make sure that the photon wavepackets share the same spatial mode, for instance by coupling the photons to an optical fibre or by placing the emitter at the focus of a parabolic mirror. The latter case allows a decomposition on co-linear plane-waves to be considered and the single-photon state can be written as:

$$|\psi\rangle = \sum_{\omega} c_{\omega}\, |1\rangle_{\omega,\varepsilon}$$

where the coefficients c_{ω} depend only on the frequency ω, and the wavevectors $|\psi\rangle$ are collinear, and:

$$\mathbf{k} = \frac{\omega}{c}\mathbf{u} \qquad \sum_{\omega} |c_{\omega}|^2 = 1$$

The quantum interference takes place when all the c_{ω} are the same for all photon wavepackets as described in ref. 15. In practice, the coupling of the exciton to the solid-state environment leads to pure dephasing, resulting in a partial mixture of the state[99]. The first HOM measurements on QD sources were reported in 2001 with indistinguishabilities M in the 70–80% range[100] (Fig. 2a,b). Since then, the community has conducted in-depth studies of what limits the indistinguishability, identifying various phenomena: fluctuating charges in the emitter vicinity; vibration of the crystal, that is, phonons; and time jitter in the carrier creation process. We briefly review these, and how to minimize their effects.

Pure dephasing. The total dephasing rate of an optical transition is given by $\gamma = (\gamma_{dec}/2) + \gamma^{*}$, where γ_{dec} is the population decay rate (due to radiative or non-radiative processes) and γ^{*} is the pure dephasing rate induced by the solid-state environment (phonons, charge noise, and so on). The indistinguishability is given by $M = \gamma_{sp}/(\gamma_{sp} + 2\gamma^{*})$, where γ_{sp} is the spontaneous emission rate. A typical example of such pure dephasing is the one induced by the phonon bath: virtual transitions involving two phonons of the same energy, one absorbed and one emitted but with different wavevectors, contribute to a temperature-dependent pure dephasing[101–104]. Fluctuating charges around the QD can also create a fluctuating electric field modifying the transition frequency through the confined Stark effect. Similarly, randomly oriented nuclear spins create a fluctuating magnetic field at the QD location, resulting in spin noise that can exceed the charge noise for the negatively charged exciton transition[105]. When the timescale of these fluctuations is faster than the temporal duration of the wavepacket, it leads to pure dephasing[106]. A solution to minimize the effect of pure dephasing is to increase γ_{sp}, by coupling the QD to a cavity mode in the regime of the Purcell effect. This tool has proven efficient to maintain a high indistinguishability[107,108].

Phonon sidebands. The interaction between the electrons and phonons also gives rise to phonon-assisted emission processes, where a photon is emitted while an acoustic phonon is absorbed or emitted. The QD emission spectrum thus consists of a narrow line (the zero-phonon line) on top of a broad emission, typically a few nanometres for InGaAs QDs (the phonon sideband)[109,110]. Such broad incoherent emission limits the indistinguishability of the emitted photon and can represent 10% of the emission for InGaAs QDs at 4 K. Spectral filtering of the QD zero-phonon line is sometimes used to obtain high indistinguishability[104]. However, inserting the QD in a cavity to accelerate the emission into the zero-phonon line can strongly reduce the phonon sideband emission without filtering[108,111].

Time jitter induced by the excitation. While experimentally convenient, the creation of high-energy carriers (Fig. 1e) limits the indistinguishability, especially at high excitation powers. The radiative cascade leading to the exciton state results in a temporal uncertainty on the photon emission[86] and a reduction of the indistinguishability when increasing the excitation power[112] (Fig. 3c). Even at low power, when a single exciton is created, the scattering time of the carriers to the QD ground state limits the indistinguishability; a limitation that is even more relevant when accelerating the exciton spontaneous emission using a cavity[99] (Fig. 2d). Such considerations have led to strictly resonant pumping schemes. The experimental challenge is then to remove the excitation laser light from the emission: this can be done by spatially decoupling the excitation from collection[80,81,113] or by using a crossed polarization configuration[83,88,114,115].

Spectral diffusion. When the charge and spin fluctuations occur on a timescale exceeding the radiative lifetime, they lead to spectral wandering of the emission energy from one photon to the other: the indistinguishability depends on the time delay Δt between emitted photons. Charge noise can be more prominent in light extraction structures such as microcavities and nanowires, because of free surfaces and associated surface states[112,116]. In high-quality bulk samples—with a very low density of traps—noise spectra reveal that charge noise dominates at low frequency (typically up to 10 Hz) while spin noise dominates at higher frequency (typically below 10 kHz)[105]. Linewidth measurements obtained by scanning a laser across the QD transition at various frequencies show radiatively limited linewidths above 50 kHz (ref. 117) (Fig. 2c), so highly indistinguishable photons could be obtained for delays as large as $\Delta t = 20$ μs.

With a clear understanding of these phenomena and the development of mitigation techniques, near-unity indistinguishable photons are now reproducibly demonstrated with InGaAs QDs. In 2013, near-unity indistinguishability was first obtained under strictly resonant pulsed excitation, at 4.2 K, filtering the zero-phonon line, with an indistinguishability corrected from $g^{(2)}(0)$ (see Box 1) of $M^{*} = 0.97\pm0.002$ (ref. 83). A temporal shaping for the resonant excitation pulse to reach rapid-adiabatic passage brought this value to $M^{*} = 0.995\pm0.007$ (ref. 88). In 2016, high indistinguishabilities were reported for single QDs in cavities[33,89] for delays up to $\Delta t = 14.7$ μs (refs 118,119). As explained below, these cavities also allow for high extraction efficiency.

Bright QD single-photon sources

Because of the high refractive index of GaAs, $n_s \approx 3.5$, the light emitted by a QD exits the semiconductor with a probability of only $\frac{1}{4}n_s^2 \approx 2\%$ from one facet. A high brightness at the output of the device—that is, at the first lens B_{lens} (Fig. 3a)—is thus the very first challenge that the community has addressed[120].

Brightness at the first lens. High brightness at the first lens can be obtained by engineering the electromagnetic vacuum field around the QD in an optical cavity or waveguide[121] to control the emission rate and pattern. The spontaneous emission rate can be enhanced into a target optical mode[122], suppressed in all others[123], or both. This leads to a preferential emission into a target mode with probability $\beta = \Gamma_{mode}/(\Gamma_{mode} + \Gamma_{others})$, where Γ_{mode} (Γ_{others}) is the emission rate into the target mode (all other modes). The probability of collecting a photon from the target mode into an optical lens is denoted η_{lens} and the probability

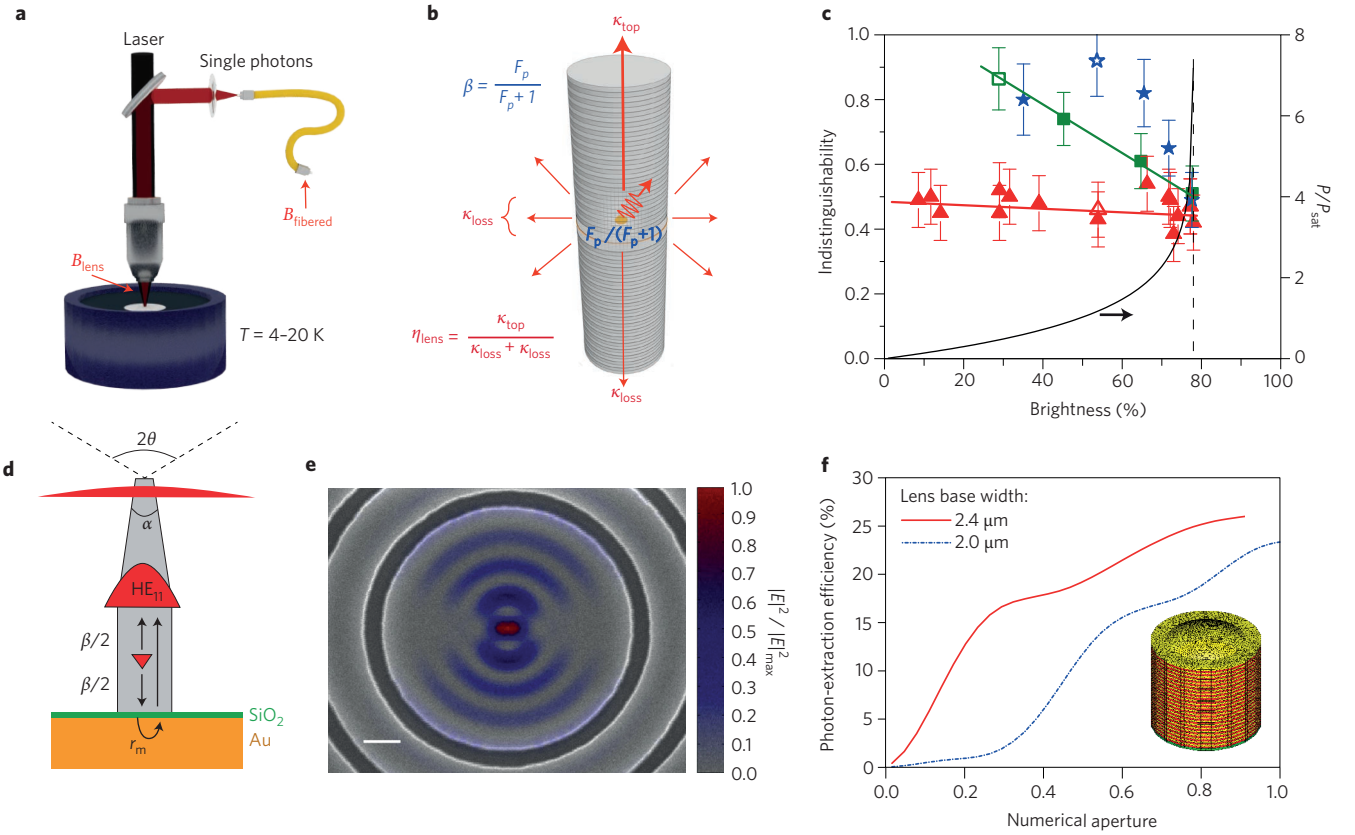

Figure 3 | Extracting single photons. a, Schematic of a QD-based experiment: the QD is inserted in a cryostat typically operating between 4 and 30 K. The QD emission is collected through a microscope objective that also allows focusing of the excitation laser. The positions where the brightness at the first lens and the fibered brightness are measured are indicated. **b**, Schematic of a pillar microcavity used to collect single photons. A QD located at the centre of the pillar cavity experiences an enhanced spontaneous emission rate by a factor F_p. The extraction into the first lens is given by the product $\beta\eta_{lens}$ (see text). **c**, Demonstration of bright sources of indistinguishable photons reported in ref. 112. The indistinguishability of the source is plotted as a function of brightness for three excitation conditions: red, excited state excitation; green, wetting layer excitation; blue, two-colour excitation (see text for more details). The dependence of the brightness on the excitation power P is indicated by the black line (right scale), where P_{sat} is the saturation power. **d**, Schematic of an etched tapered nanowire deposited on a gold mirror embedding a QD. The tapering angle α is precisely adjusted to allow an efficient collection into the first lens and a dielectric layer is inserted between the nanowire and the mirror to limit losses. r_m is the lower mirror reflectivity and HE_{11} refers to the guided mode. **e**, Scanning electron microscopy of a circular Bragg grating bulls-eye cavities and a simulated intensity map of the electric field, E. The scale bar represents 200 nm. **f**, Calculated extraction efficiency of a microlens structure as a function of the first lens numerical aperture for various lens base widths. Panels adapted from: **c**, ref. 112, Macmillan Publishers Ltd; **f**, ref. 160, Macmillan Publishers Ltd. Panels reproduced from: **d**, ref. 147, Macmillan Publishers Ltd; **e**, ref. 158, Macmillan Publishers Ltd.

of each photon being collected at the first lens is thus the extraction efficiency $\beta\eta_{lens}$. It is a figure of merit for the photonic structure.

Naturally, the brightness also depends on the probability that the QD emits a photon. Ideally, the QD is initialized in a well-defined state with probability p_{state} close to unity at saturation power. However, if traps are in the QD vicinity, or if the QD is inserted in a gated structure, blinking of the QD can be observed between a charged and neutral exciton state, reducing the saturation value for p_{state}. Finally, the radiative emission probability is described by the quantum efficiency η_{QE} of the transition, which can be reduced because of processed surfaces.

Overall, the brightness at the first lens is $B_{lens} = \beta\eta_{lens}p_{state}\eta_{QE}$. After a decade of fundamental studies and technological developments, various photonic structures such as cavities and waveguides have been used to achieve $B_{lens} \approx 60$–80%.

Cavity-based sources. First demonstrated for atoms[124], the control of spontaneous emission of QDs was demonstrated in the late 90s and early 2000s with small mode-volume cavities fabricated using III–V semiconductor processing techniques. Acceleration of spontaneous emission was first demonstrated for QD ensembles[122] and then for single QDs in micropillar[120,125], microdisk[126] and photonic-crystal cavities[127], eventually reaching the strong-coupling regime[128–130]. The QD–cavity coupling is characterized by the light matter interaction $g \propto \sqrt{(f/V)}$ where f is the optical transition oscillator strength and V is the cavity mode effective volume. In the weak-coupling regime, the emission rate into the cavity mode is $\Gamma_{mode} = 4g^2/\kappa$ with κ the photon escape rate outside the cavity, inversely proportional to the mode quality factor Q. The Purcell factor $F_P = \Gamma_{mode}/\gamma$ scales as Q/V and characterizes the acceleration of the spontaneous emission into the cavity mode with respect to emission rate in bulk γ (ref. 131).

Bright sources have been obtained using micropillar cavities where the optical field is confined vertically by two distributed Bragg mirrors and laterally by the high refractive index contrast. The mode volume is of the order of few λ^3 and the quality factor can reach values[132,133] of a few 10^5. In such cavities, the emission rate in other modes is roughly unchanged[122] so that $\beta \approx F_P/(F_P+1)$. Lateral confinement can also be obtained through controlled lateral oxidation leading to a low refractive index layer[134]. For micropillars with typical lateral size around 2–4 μm, the fundamental mode radiation pattern is highly directive and can be collected with a standard numerical aperture around 0.5. η_{lens} is then given by the ratio

Table 1 | Characteristics of QD-based single-photon sources.

Reference	Photonic structure	Lifetime (ns)	Spectral filtering	Non-resonant excitation Unpolarized brightness			Resonant excitation Polarized brightness		
				B_{lens}	$g^{(2)}(0)$	M/M^*	B_{lens}	$g^{(2)}(0)$	M/M^*
147	Tapered nanowire	2.4	No	0.72±0.09	<0.008	–	–	–	–
155	Nano-trumpet	0.82	No	0.75±0.10	0.31 0.25*				
112	Micropillar	0.265–0.270	Yes	0.79±0.08 0.53±0.05	0.05	0.55±0.05† 0.92±0.10†	–	–	–
138	Adiabatic pillar	0.14±0.04	Yes	0.74±0.05	0.10 ±0.03	0.75±0.05†	–	–	–
160	Microlens	~1	No	0.23±0.03	<0.01*	0.80±0.07†			
158	Bulls-eye cavities	0.52	No	0.48±0.05	0.009±0.005	–			
141	Photonic crystal cavities	1.61	Yes	0.443±0.021	0.04±0.05	0.13±0.02†			
33	Connected pillar	0.08–0.12	Yes	0.65±0.07	0.024±0.007	0.74±0.07 0.78±0.07†	0.154±0.015	0.0028±0.0012	0.989±0.004 0.9956±0.0045†
89	Micropillar	0.084	Yes	–	–	–	0.33‡	0.009±0.002	0.959±003 0.978±0.004†
90	Micropillar	0.168 ±0.005	Yes	–	–	–	0.37±0.02	0.0092±0.0004	0.73±0.01†

This table highlights state-of-the-art results for bright single-photon sources using various photonic structures for efficient collection (second column). For each study, we indicate the brightness at the first lens, $g^{(2)}(0)$ and indistinguishability at saturation. The inverse of the photon lifetime (third column) gives an upper bound to maximum repetition rate at which the source can be operated. Two types of operations are considered: non-resonant excitation where the given brightness is unpolarized, and resonant excitation where the brightness is polarized. We also indicate whether the device provides spectral selection in the operation without additional filtering. 'No' means that an additional spectral filtering is necessary. In this case, the indicated brightness does not include the losses related to this necessary spectral selection. Uncertainties have been listed where included in the original paper. *Background-corrected values. †$g^{(2)}(0)$-corrected values, M^*. ‡This value is deduced considering that the crossed polarization collection scheme reduces the reported stated brightness of 66% by a factor of two.

of the cavity-photon escape rate towards the top, normalized to the total escape rate—including losses to the substrate and sidewalls — $\eta_{lens} = \kappa_{top}/(\kappa_{top} + \kappa_{loss})$ (Fig. 3b).

Brightness was not evaluated in early QD microcavity structures[125,135] until $B_{lens} \approx 38\%$ was reported in 2007 with oxidized cavities[136], followed by similar performances in electrically controlled micropillar structures[137]. In 2013, with a deterministic device fabrication where QDs with $p_{state} \approx 1$ were positioned at the centre of micropillar cavities, brightnesses at the first lens between $B_{lens} \approx 55\%$ and $B_{lens} \approx 79\%$ were reported on several devices. To maximize the outcoupling efficiency, the planar cavity quality factor, determining κ_{top} and the pillar size governing κ_{loss} were chosen to obtain $\eta_{lens} > 0.90$. High brightness was combined with $M^* = (0.5\pm0.05)$–(0.92 ± 0.1). M was shown to decrease with brightness under non-resonant excitation, due to increased time jitter and charge noise. Quasi-resonant excitation in a QD excited state showed brightness-independent $M^* \approx 0.5$, limited by charge noise. A two-colour excitation scheme, combining a very low power non-resonant excitation with the pulsed quasi-resonant excitation demonstrated $M^* \approx 0.92\pm0.1$ at $B_{lens} = 52\pm5\%$ (Fig. 3c). Similar performances were obtained in a strong Purcell effect regime[138] where $\beta\eta_{lens} \approx 0.9$ using an adiabatic cavity design[139], allowing a higher repetition rate.

Photonic-crystal cavities have also been extensively studied[127,128,140]. Compared with micropillar cavities, photonic-crystal cavities provide strong optical confinement with $V \approx 0.1$–$0.3\lambda^3$ as well as inhibition of spontaneous emission into the other modes with $\Gamma_{others} \approx 0.1\gamma$ leading to near unity β. Photonic-crystal structures are mostly studied for fully integrated approaches for on-chip optical manipulation with integrated sources. One challenge is to efficiently couple the cavity mode to an integrated waveguide—equivalent to η_{lens} for the free-space approach—with low off-chip losses. Engineering the free-space mode profile of a photonic-crystal cavity can also be done with $B_{lens} \approx 34\%$ recently demonstrated with some indistinguishability[141].

When using a cavity to collect single photons, the detuning between the QD and the cavity resonance must be adjusted. This can be achieved by adjusting the temperature as the electronic bandgap (determining the QD resonance) and the refractive index (determining the cavity resonance) have different dependences[129,130]. However, increasing the temperature favours phonon-assisted decoherence and is detrimental to indistinguishability[104]. A better solution consists in applying an electric field and tuning the QD transition through the confined d.c. Stark effect[142,143]. Oxidation-based cavity structures inspired from laser technologies are well suited for defining electrical contacts[136]. For micropillars, two approaches have proven successful: define an annular contact on top of micropillars[144] or connect the pillar to a bigger frame through one-dimensional ridges[145].

Waveguide-based sources. Efficient collection can also be obtained with single-mode waveguides defined either in plane or out of plane[146–151]. Developed simultaneously for defects in diamond[152] and self-assembled QDs[146,147], this approach relies on spontaneous-emission inhibition in all modes except one[153], typically with $\Gamma_{others} \approx 0.1\gamma$. Explored with both for photonic crystal-based waveguides[146,149,151] and nanowires[147,148] (off-chip), with β exceeding 0.9 (refs 146,153). In the former, enhanced spontaneous-emission rate can also be reached using slow modes[146,154]. To collect photons in one direction only, half-waveguides are defined with photonic crystals and a metallic mirror spaced by a dielectric layer added at the end of nanowires[147]. For off-chip collection, η_{lens} is optimized by minimizing diffraction at the nanowire end through progressive tapering (needle shape in Fig. 3d). In 2010, Claudon and co-workers demonstrated $B_{lens} \approx 72\%$ for top-down processed tapered nanowires[147]

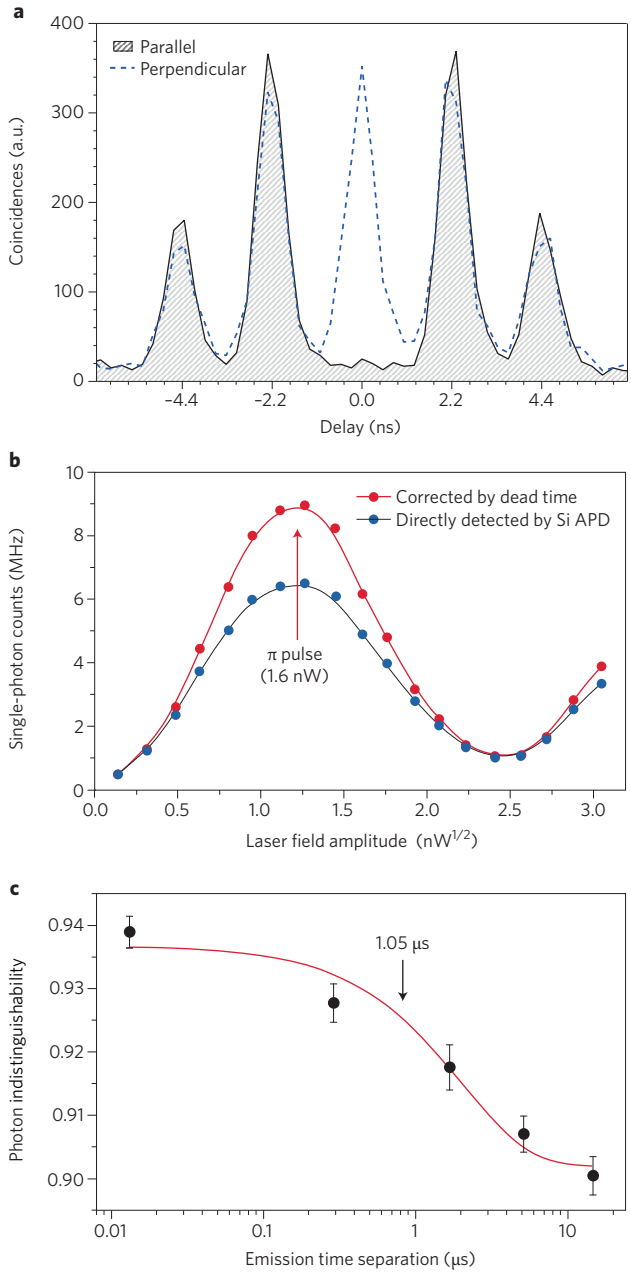

Figure 4 | State of play. a, HOM measurement obtained under resonant fluorescence showing the total suppression of the zero delay peak for parallel polarized photons (measurement scheme similar to Fig. 2b, but here only the centre five peaks are shown). The indistinguishability is $M^* = 0.995 \pm 0.0045$ for a brightness at the first lens of 16% for polarized light — measurement was obtained on a deterministically coupled connected-pillar cavity. **b**, Count rate detected at the output of a single mode fibre (blue) and corresponding count rate corrected from the detector dead time (red) as a function of the excitation power. The 9 MHz count rate obtained at π pulse under 76 MHz excitation rate, corrected from the 32% avalanche photodetector (APD) efficiency, corresponds to $B_{SMF} = 0.37$. **c**, Study of the photon indistinguishability as a function of the emission-time separation of the photon showing the generation of highly indistinguishable photons over long temporal separations (measurements obtained on a randomly fabricated QD pillar-cavity device). Panel **a** adapted from ref. 33, Macmillan Publishers Ltd. Panels **b** and **c** reproduced from ref. 163, Macmillan Publishers Ltd.

with a numerical aperture of 0.7. Later, bottom-up grown nanowires[148] showed $B_{lens} \approx 42\%$. More recently, reversed tapering leading to nano-trumpet shapes was shown to be more robust to nanofabrication uncertainties and allowed $B_{lens} \approx 76\%$ (ref. 155). Because enhancement of the spontaneous emission rate is small and QDs are close to etched surfaces, the indistinguishability is still limited.

Other approaches. Metallic-dielectric structures such as Tamm-confined modes[156] or silver-based nanocavities[157] have been developed, although collection is ultimately limited by metallic losses. Circular Bragg-grating bulls-eye cavities deterministically etched around a targeted QD in a GaAs suspended membrane (Fig. 3e) show strong field confinement[158], a broadband enhancement of spontaneous emission, $F_P = 3$ and $B_{lens} \approx 48\%$. Microlenses etched in the semiconductor on top of a QD[159,160] show photon extraction similar to a solid-immersion lens without the Purcell effect. A mirror below the microlens increases the emission towards the top (Fig. 3f) showing $B_{lens} \approx 23\%$ with a Bragg mirror.

Table 1 summarizes the current state of the art for brightness at the first lens for both non-resonant excitation (with the excitation laser wavelengths detuned from the QD emission) and strictly resonant excitation. A brightness in the first lens close to 80% has now been repeatedly demonstrated[112,147,155,161] combined with a high degree of indistinguishability of approximately 75% for pillar-based cavities[33,112,138] limited by time jitter induced by the charge capture[99]. Resonant excitation on pillar cavities showed near-unity indistinguishability with $M^* > 0.98$ (refs 33,89; see Fig. 4a). So far, this was obtained with resonant excitation exciting the cavity from the top and the excitation laser light being suppressed in a crossed-polarization configuration. Thus, the single photon presents a linear polarization, and the brightness is limited to half the extraction efficiency. To go beyond this limitation, side excitation schemes could be implemented to separate the excitation from collection[113].

Beyond the brightness at the first lens. A useful brightness for an end-user is typically desired at the output of a single mode fibre (SMF). B_{SMF} depends on B_{lens} as well as on the coupling efficiency into the fibre. In many structures discussed above—pillar cavities[162], microlenses[160], nanowires[150,155]—the mode profile has a good overlap with the mode of a SMF. To date, there have been only a few results addressing the fibered brightness[118,119]. A high single-photon purity—$g^{(2)}(0) \approx 0.028$—was demonstrated for $B_{SMF} = 0.14$, yielding more than 3.6×10^6 counts per second on a silicon avalanche photon detector, and corresponding to $\sim10^7$ photons per second from a 82 MHz excitation rate[118]. Similar figures were also obtained for resonantly excited micropillars, with 1.6×10^6 counts per second measured for very high indistinguishability[119]. Most recently, a record value of $B_{SMF} = 0.37$ (Fig. 4b) for an indistinguishability above 0.9 was reported (Fig. 4c)[163]. Note that a high single-photon purity, $g^{(2)}(0) \approx 0.055$ and $B_{SMF} = 0.058$ were also obtained for InAs/InP QDs sources operating at 1.55 μm (ref. 164).

Built-in spectral filtering. For non-resonant excitation, high brightness is obtained at saturation power where $p_{state} \approx 1$. The QD emits a cascade of photons and a single photon is obtained only through spectral filtering one emission line over several separated in wavelength by a few nanometres. High-quality-factor microcavities provide simultaneously an efficient photon collection and the necessary spectral filtering of the transition of interest[118]. Nanowires, photonic-crystal waveguides, bulls-eye cavities or microlenses provide spectrally broad photon extraction which—while beneficial for some applications—requires narrow-band filters after the device. The built-in spectral filtering of the device is indicated in Table 1.

Operation rate. Finally, the temporal duration of the photon wavepacket puts an upper bound on the source operation rate. Nanowires have a temporal duration of the photon wavepacket of 2–4 ns, while high-Purcell-factor cavities generate highly

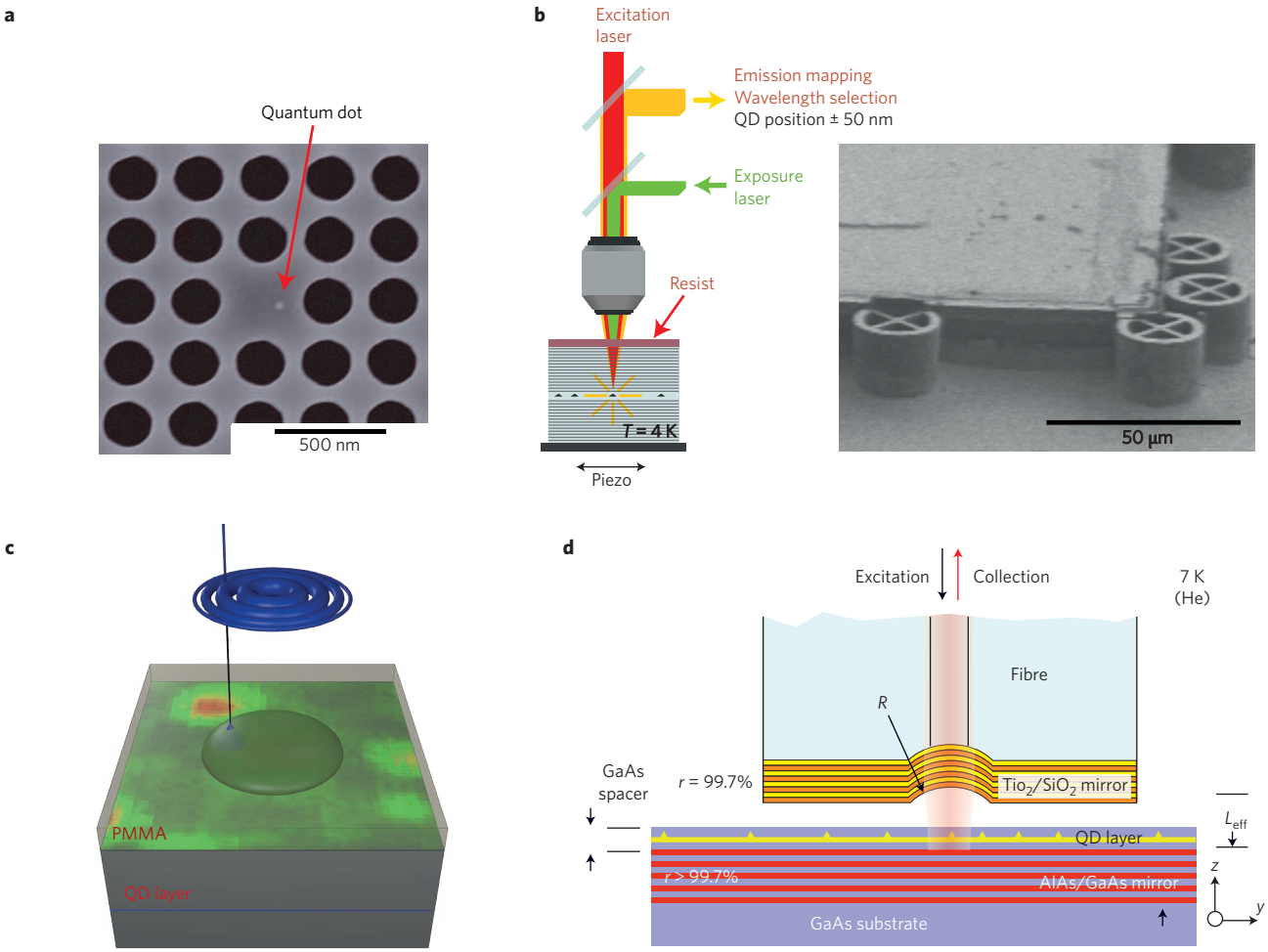

Figure 5 | Deterministic device fabrication. a, First demonstration of the positioning of a single QD in a photonic-crystal cavity. The technique is based on measuring the QD position with respect to marks through atomic force or scanning electron microscopy, then constructing the cavity around it through processing. **b**, Left: schematic of the *in situ* lithography[168] technique, which allows a micropillar cavity to be constructed around a QD. The QD position is measured through mapping the emission intensity and a cavity is exposed in a photoresist centred on the QD with a green laser line. Right: scanning electron microscopy image of four connected pillar cavities[33] each embedded with a QD within 50 nm from the pillar centre. **c**, Principle of e-beam *in situ* lithography, which defines a microlens on top of a QD. The QD position is measured by monitoring the cathodoluminescence signal. The lens shape is obtained in the lithography process. PMMA stands for poly(methyl methacrylate) and is an electronic resist. **d**, Schematic of cavities based on a movable micro-mirror defined at the end of a fibre. The cavity is formed through a second Bragg mirror grown below the QD layer. The sample is precisely positioned below the micro-mirror and the cavity length is tuned to match the QD resonance. *r* is the reflectivity of the mirror, *R* is the radius of curvature and L_{eff} is the effective cavity length. Panels reproduced from: **a**, ref. 166, AAAS; **d**, ref. 175, AIP. Panel **c** adapted from ref. 160, Macmillan Publishers Ltd.

indistinguishable photons with lifetime below 0.1 ns (Table 1). With a similar brightness at the first lens, cavity-based approaches allow a maximum operation rate around 1–2 GHz, more than an order of magnitude higher than waveguide-based devices.

Deterministic device fabrication

As the community has reproducibly demonstrated the potential of QDs for efficient quantum light generation, the technological challenges for large-scale use need to be addressed. Close to unity quantum efficiency and indistinguishability have all been obtained with self-assembled QDs. Their random location has been a barrier for positioning in photonic structures. Moreover, for cavity-based devices, the QD optical transition must match the cavity resonance, yet QD ensembles are inhomogeneously spectrally broadened by around 20–70 nm for cavity linewidths below 1 nm. Without control of both the spatial and spectral position of the QD, the success rate for the fabrication of microcavity QD sources is small, ~10^{-3}–10^{-4}. However, high-yield fabrication methods are now becoming available.

The position of QDs can be controlled through sophisticated growth techniques using pre-pattern substrates[70–72]. These techniques have successfully been used to position QDs in cavities with nanometre accuracy[71,73,165]. Site-controlled growth of QDs in nanowires can be achieved, allowing a deterministic positioning at the centre of the waveguide[148]. In both cases, the indistinguishability of the emitted photons has so far remained limited.

To benefit from the high optical quality of self-assembled QDs, defining a photonic structure around randomly positioned QDs was pioneered in 2005. The QD position was measured through scanning electron microscopy imaging using metallic marks that were used to process a photonic-crystal cavity around the QD (Fig. 5a)[166]. The cavity resonance was then brought close to the QD resonance by multiple digital etching steps. The method was further improved to reach the strong coupling regime[167]. In 2008, another technique was proposed based on a cryogenic photolithography performed on a planar cavity embedding randomly positioned QDs. The QD positions are measured optically by imaging their emission pumped

with a laser and a second laser line, aligned to the first, is used to define a pattern precisely centred on the QD (Fig. 5b)[168]. Adopted by several groups[90,169,170], the technique was used to define pillar QD devices both in the weak[168] and strong-coupling regime[171]. It was improved to fabricate pillar devices with an electrical bias for fine-tuning of the QD cavity spectral resonance[145] with pillars connected through ridges to a large mesa where an electrical contact is defined.

Emission scanning approaches have also been used to measure the QD position with respect to metallic marks, or to define marks using cryogenic *in situ* lithography[158,172,173]. Photonic-crystal[173] or bulls-eye[158] cavities are then defined through e-beam lithography aligned to the marks. An *in situ* e-beam lithography has also been developed, where cryogenic cathodoluminescence is used to measure the QD position at low electron dose, and the resist is exposed at high dose to define microlenses centred on QDs[159,160] (Fig. 5c).

A different approach—first demonstrated with rubidium atoms[174]—is based on a cavity with one external mirror formed at the end of an optical fibre, and one epitaxial distributed Bragg reflector (DBR) mirror on which a partial cavity region containing QDs is formed (Fig. 5d). The cavity resonance is tunable by adjusting the fibre–semiconductor distance, and QD emission is directly coupled into the fibre[175,176]. Because of mode-matching issues, this approach has been extended to a flat silica external mirror[177].

State of play and future challenges

There have been roughly two and a half decades of research and development of III–V QD structures for optical applications. The initial period of the early 1990s to 2000 focused on fundamental crystal growth, cavity quantum electrodynamics with QD ensembles, and initial single-emitter measurements. In the past decade, deep understanding of the physics at play and the coupling to photonic structures improved the source indistinguishability and brightness. The result is a new generation of bright sources of pure and indistinguishable single photons. Especially because of their unprecedented brightness, these single-photon sources are expected to enable a new generation of fundamental research in quantum optics and quantum engineering.

For applications in some areas, such as short-distance quantum communication, quantum metrology[178] or quantum imaging[179], that rely on single-photon purity but not on indistinguishability, single-photon sources with an external brightness in the 80% range are now available using QDs in nanowires[147,148], nano-trumpets[155] or micropillar cavities[33,89,90,112]. Using deterministic processing, pillar cavity devices can now be fabricated with a very high yield[90,112,145,168].

When indistinguishable single photons are required, SPDC sources provide heralded single photons with a high degree of indistinguishability, but at the cost of a brightness limited to typically 2% (Fig. 1b,c). QD devices can now deliver single-photon sources with near unity indistinguishability, high single-photon purity — $g^{(2)}(0) < 2\%$—and a brightness in the 15–30% range[33,89]. This was obtained by combining high acceleration of spontaneous emission, $F_p > 10$, to limit dephasing[107] and resonant excitation to suppress the time jitter[99]. High brightness at the output of a single mode fibre has recently been demonstrated showing the full potential of the developed device[89,118,163].

One way to take advantage of recent progress is to use single photons successively generated by a bright QD source and actively spatially route the photons into different optical paths—demultiplexing—provided that photons remain indistinguishable even if generated at long time delays. Many experiments have tested the indistinguishability of photons generated a few nanoseconds apart. However, spectral diffusion at longer delays can reduce the spectral overlap of photons emitted at different times. The indistinguishability of QDs in microlenses rapidly decreases for delays as short as $\Delta t = 20$ ns (ref. 104). However, micropillar devices have shown highly indistinguishable photons (>90%) over microsecond timescales[118,119] (Fig. 4c).

Very recently, using either passive, inefficient demultiplexing based on beamsplitters or efficient active demultiplexing, QD-based sources have been used to implement three- to five-photon boson sampling measurements much faster that their SPDC counterpart implementation. The achieved rates are between one[180] (for three photons) and five (for five photons) orders of magnitude higher than current heralded multi-photon sources based on SPDC[163].

Future steps should ensure the full scalability of QD-based single-photon sources for quantum technologies. An important step is the generation of indistinguishable photons from distant sources. First demonstrations of quantum interference between two photons generated by distinct QDs have been reported in 2010 for non-resonantly excited QDs using controlled strain[77] or electrical bias[181] to tune the two QDs. More recently, such quantum interference was reported for bright single-photon sources[138]. In these studies, the indistinguishability for two sources was mostly limited by the single-source indistinguishability. However, using strictly resonant excitation, the quantum interference for photons from two QDs was shown to reach high visibility[182], around 82%. Thus, we expect that a high degree of indistinguishability will be achieved for resonantly driven remote bright single-photon sources.

State-of-the-art single-photon sources now operate in the 900–970 nm range based on the very mature growth of InGaAs/GaAs self-assembled QDs. Developing sources at shorter wavelengths will allow QDs devices to be integrated with atomic-based quantum devices to access long-lifetime atomic memories. Recently, single photons emitted by GaAs/AlAs QDs grown by droplet epitaxy have been coupled to an atomic-vapour memory[183]. For long-distance applications, high-quality single photons at telecom wavelengths will be necessary. A bright single-photon source ($B_{lens} \approx 36\%$) has recently been obtained at 1.3 μm, yet with limited indistinguishability[184]. Single-photon sources have also been reported at 1.55 μm, leading to demonstration of quantum key distribution over up to 120 km (refs 164,185). An alternative is to fabricate the best single-photon source at one wavelength and frequency convert the single photon to the desired wavelength. Efficient frequency conversion has been demonstrated at various wavelengths including 1.55 μm (refs 186–188) and was also used to erase the energy difference between two QDs[187]. High external-conversion efficiencies, above 40%, have been demonstrated using bulk PPLN (periodically poled lithium niobate) nonlinear crystals[187] and frequency-conversion devices have now been developed in an integrated semiconductor platform[28].

Received 19 July 2016; accepted 29 September 2017; published online 7 November 2017

References

1. Dowling, J. P. & Milburn, G. J. Quantum technology: the second quantum revolution. *Phil. Trans. R. Soc. A* **361,** 1655–1674 (2003).
2. Braunstein, S. L. Squeezing as an irreducible resource. *Phys. Rev. A* **71,** 055801 (2005).
3. Gisin, N., Ribordy, G., Tittel, W. & Zbinden, H. Quantum cryptography. *Rev. Mod. Phys.* **74,** 145–195 (2002).
4. Bao, N. & Halpern, N. Y. Quantum voting and violation of Arrow's impossibility theorem. *Phys. Rev. A* **95,** 062306 (2017).
5. Giovannetti, V., Lloyd, S. & Maccone, L. Quantum metrology. *Phys. Rev. Lett.* **96,** 010401 (2006).
6. Dowling, J., Gatti A. & Sergienko, A. (eds) Quantum imaging. *J. Mod. Opt.* **53,** 5–6 (2006).
7. Lloyd, S. Universal quantum simulators. *Science* **273,** 1073–1078 (1996).
8. Knill, E., Laflamme, R. & Milburn, G. J. A scheme for efficient quantum computation with linear optics. *Nature* **409,** 46–52 (2001).
9. Jozsa, R. & Linden, N. On the role of entanglement in quantum-computational speed-up. *Proc. R. Soc. A.* **459,** 2011–2032 (2003).
10. Vidal, G. Efficient classical simulation of slightly entangled quantum computations. *Phys. Rev. Lett.* **91,** 147902 (2003).
11. Nielsen, M. A. & Chuang, I. L. *Quantum Information, Computation and Communication* (Cambridge Univ. Press, 2010).

12. Natarajan, C. M., Tanner, M. G. & Hadfield, R. H. Superconducting nanowire single-photon detectors: physics and applications. *Supercond. Sci. Technol.* **25,** 063001 (2012).
13. Carolan, J. *et al.* Universal linear optics. *Science* **349,** 711–716 (2015).
14. Volz, J., Scheucher, M., Junge, C. & Rauschenbeutel, A. Nonlinear π phase shift for single fibre-guided photons interacting with a single resonator-enhanced atom. *Nat. Photon.* **8,** 965–970 (2014).
15. Grynberg, G., Aspect, A. & Fabre, C. *Introduction to Quantum Optics: From the Semi-classical Approach to Quantized Light* (Cambridge Univ. Press, 2010).
16. Brassard, G., Lütkenhaus, N., Mor, T. & Sanders, B. C. Limitations on practical quantum cryptography. *Phys. Rev. Lett.* **85,** 1330–1333 (2000).
17. Broome, M. A. *et al.* Photonic boson sampling in a tunable circuit. *Science* **339,** 794–798 (2013).
18. Spring, J. B. *et al.* Boson sampling on a photonic chip. *Science* **339,** 798–801 (2013).
19. Spagnolo, N. *et al.* Experimental validation of photonic boson sampling. *Nat. Photon.* **8,** 615–620 (2014).
20. Tillmann, M. *et al.* Experimental boson sampling. *Nat. Photon.* **7,** 540–544 (2013).
21. Hong, C. K., Ou, Z. Y. & Mandel, L. Measurement of subpicosecond time intervals between two photons by interference. *Phys. Rev. Lett.* **59,** 2044–2046 (1987).
22. Jin, R.-B. *et al.* Efficient detection of an ultra-bright single-photon source using superconducting nanowire single-photon detectors. *Opt. Commun.* **336,** 47–54 (2015).
23. Wang, X.-L. *et al.* Experimental ten-photon entanglement. *Phys. Rev. Lett.* **117,** 210502 (2016).
24. Burnham, D. C. & Weinberg, D. L. Observation of simultaneity in parametric production of optical photon pairs. *Phys. Rev. Lett.* **25,** 84–87 (1970).
25. Kwiat, P. G. & Chiao, R. Y. Observation of a nonclassical Berry's phase for the photon. *Phys. Rev. Lett.* **66,** 588–591 (1991).
26. Fasel, S. *et al.* High-quality asynchronous heralded single-photon source at telecom wavelength. *New J. Phys.* **6,** 163 (2004).
27. Azzini, S. *et al.* Ultra-low power generation of twin photons in a compact silicon ring resonator. *Opt. Express* **20,** 23100–23107 (2012).
28. Li, Q., Davanço, M. & Srinivasan, K. Efficient and low-noise single-photon-level frequency conversion interfaces using silicon nanophotonics. *Nat. Photon.* **10,** 406–414 (2016).
29. Kwiat, P. G., Waks, E., White, A. G., Appelbaum, I. & Eberhard, P. H. Ultrabright source of polarization-entangled photons. *Phys. Rev. A* **60,** R773–R776 (1999).
30. U'Ren, A. B., Silberhorn, C., Banaszek, K. & Walmsley, I. A. Efficient conditional preparation of high-fidelity single photon states for fiber-optic quantum networks. *Phys. Rev. Lett.* **93,** 093601 (2004).
31. Harder, G. *et al.* An optimized photon pair source for quantum circuits. *Opt. Express* **21,** 13975–31985 (2013).
32. Barbieri, M. *et al.* Parametric downconversion and optical quantum gates: two's company, four's a crowd. *J. Mod. Opt.* **56,** 209–214 (2009).
33. Somaschi, N. *et al.* Near-optimal single-photon sources in the solid state. *Nat. Photon.* **10,** 340–345 (2016).
34. Pan, J.-W. *et al.* Multiphoton entanglement and interferometry. *Rev. Mod. Phys.* **84,** 777–838 (2012).
35. Barbieri, M. Effects of frequency correlation in linear optical entangling gates operated with independent photons. *Phys. Rev. A* **76,** 043825 (2007).
36. Brańczyk, A. M., Fedrizzi, A., Stace, T. M., Ralph, T. C. & White, A. G. Engineered optical nonlinearity for quantum light sources. *Opt. Express* **19,** 55–65 (2011).
37. Weston, M. M. *et al.* Efficient and pure femtosecond-pulse-length source of polarization-entangled photons. *Opt. Express* **24,** 10869–10879 (2016).
38. Migdall, A. L., Branning, D. & Castelletto, S. Tailoring single-photon and multiphoton probabilities of a single-photon on-demand source. *Phys. Rev. A* **66,** 053805 (2002).
39. Xiong, C. *et al.* Active temporal multiplexing of indistinguishable heralded single photons. *Nat. Commun.* **7,** 10853 (2016).
40. Mendoza, G. J. *et al.* Active temporal and spatial multiplexing of photons. *Optica* **3,** 127–132 (2016).
41. Kimble, H. J., Dagenais, M. & Mandel, L. Photon antibunching in resonance fluorescence. *Phys. Rev. Lett.* **39,** 691–695 (1977).
42. Diedrich, F. & Walther, H. Nonclassical radiation of a single stored ion. *Phys. Rev. Lett.* **58,** 2013–2016 (1987).
43. Basché, T., Moerner, W. E., Orrit, M. & Talon, H. Photon antibunching in the fluorescence of a single dye molecule trapped in a solid. *Phys. Rev. Lett.* **69,** 1516–1519 (1992).
44. Michler, P. *et al.* A quantum dot single-photon turnstile device. *Science* **290,** 2282–2285 (2000).
45. Gammon, D., Snow, E. S., Shanabrook, B. V., Katzer, D. S. & Park, D. Homogeneous linewidths in the optical spectrum of a single gallium arsenide quantum dot. *Science* **273,** 87–90 (1996).
46. Sebald, K. *et al.* Single-photon emission of CdSe quantum dots at temperatures up to 200 K. *Appl. Phys. Lett.* **81,** 2920–2922 (2002).
47. Couteau, C. *et al.* Correlated photon emission from a single II–VI quantum dot. *Appl. Phys. Lett.* **85,** 6251–6253 (2004).
48. Holmes, M. J., Choi, K., Kako, S., Arita, M. & Arakawa, Y. Room-temperature triggered single photon emission from a III-nitride site-controlled nanowire quantum dot. *Nano Lett.* **14,** 982–986 (2014).
49. Michler, P. *et al.* Quantum correlation among photons from a single quantum dot at room temperature. *Nature* **406,** 968–970 (2000).
50. Mahler, B. *et al.* Towards non-blinking colloidal quantum dots. *Nat. Mater.* **7,** 659–664 (2008).
51. Faraon, A., Barclay, P. E., Santori, C., Fu, K.-M. C. & Beausoleil, R. G. Resonant enhancement of the zero-phonon emission from a colour centre in a diamond cavity. *Nat. Photon.* **5,** 301–305 (2011).
52. Schukraft, M. *et al.* Precision nanoimplantation of nitrogen vacancy centers into diamond photonic crystal cavities and waveguides. *APL Photon.* **1,** 020801 (2016).
53. Riedrich-Möller, J. *et al.* One- and two-dimensional photonic crystal microcavities in single crystal diamond. *Nat. Nanotech.* **7,** 69–74 (2012).
54. Zhong, T., Kindem, J. M., Miyazono, E. & Faraon, A. Nanophotonic coherent light–matter interfaces based on rare-earth-doped crystals. *Nat. Commun.* **6,** 8206 (2015).
55. Koperski, M. *et al.* Single photon emitters in exfoliated WSe_2 structures. *Nat. Nanotech.* **10,** 503–506 (2015).
56. Srivastava, A. *et al.* Optically active quantum dots in monolayer WSe_2. *Nat. Nanotech.* **10,** 491–496 (2015).
57. Chakraborty, C., Kinnischtzke, L., Goodfellow, K. M., Beams, R. & Vamivakas, A. N. Voltage-controlled quantum light from an atomically thin semiconductor. *Nat. Nanotech.* **10,** 507–511 (2015).
58. He, Y.-M. *et al.* Single quantum emitters in monolayer semiconductors. *Nat. Nanotech.* **10,** 497–502 (2015).
59. Aharonovich, I., Englund, D. & Toth, M. Solid-state single-photon emitters. *Nat. Photon.* **10,** 631–641 (2016).
60. Goldstein, L., Glas, F., Marzin, J. Y., Charasse, M. N. & Roux, G. L. Growth by molecular beam epitaxy and characterization of InAs/GaAs strained layer superlattices. *Appl. Phys. Lett.* **47,** 1099–1101 (1985).
61. Tabuchi, M., Noda, S. & Sasaki, A. in *Science and Technology of Mesoscopic Structures* (eds Namba, S. *et al.*) 379–384 (Springer, 1992).
62. Leonard, D., Krishnamurthy, M., Reaves, C. M., Denbaars, S. P. & Petroff, P. M. Direct formation of quantum-sized dots from uniform coherent islands of InGaAs on GaAs surfaces. *Appl. Phys. Lett.* **63,** 3203–3205 (1993).
63. Solomon, G. S., Trezza, J. A. & Harris, J. S. Effects of monolayer coverage, flux ratio, and growth rate on the island density of InAs islands on GaAs. *Appl. Phys. Lett.* **66,** 3161–3163 (1995).
64. Solomon, G. S., Trezza, J. A. & Harris, J. S. Substrate temperature and monolayer coverage effects on epitaxial ordering of InAs and InGaAs islands on GaAs. *Appl. Phys. Lett.* **66,** 991–993 (1995).
65. Wu, W., Tucker, J. R., Solomon, G. S. & Harris, J. S. Atom-resolved scanning tunneling microscopy of vertically ordered InAs quantum dots. *Appl. Phys. Lett.* **71,** 1083–1085 (1997).
66. Marzin, J.-Y., Gérard, J.-M., Izraël, A., Barrier, D. & Bastard, G. Photoluminescence of single InAs quantum dots obtained by self-organized growth on GaAs. *Phys. Rev. Lett.* **73,** 716–719 (1994).
67. Fafard, S., Leonard, D., Merz, J. L. & Petroff, P. M. Selective excitation of the photoluminescence and the energy levels of ultrasmall InGaAs/GaAs quantum dots. *Appl. Phys. Lett.* **65,** 1388–1390 (1994).
68. Watanabe, K., Koguchi, N. & Gotoh, Y. Frabrication of GaAs quantum dots by modified droplet epitaxy. *Jpn J. Appl. Phys.* **39,** L79–L81 (2000).
69. Kuroda, T. *et al.* Symmetric quantum dots as efficient sources of highly entangled photons: violation of Bell's inequality without spectral and temporal filtering. *Phys. Rev. B* **88,** 041306 (2013).
70. Schmidt, O. G. (ed.) *Lateral Alignment of Epitaxial Quantum Dots* (Springer-Verlag, 2007).
71. Schneider, C. *et al.* Single site-controlled In(Ga)As/GaAs quantum dots: growth, properties and device integration. *Nanotechnology* **20,** 434012 (2009).
72. Dalacu, D. *et al.* Directed self-assembly of single quantum dots for telecommunication wavelength optical devices. *Laser Photon. Rev.* **4,** 283–299 (2010).
73. Mohan, A. *et al.* Record-low inhomogeneous broadening of site-controlled quantum dots for nanophotonics. *Small* **6,** 1268–1272 (2010).
74. Bennett, A. J. *et al.* Electric-field-induced coherent coupling of the exciton states in a single quantum dot. *Nat. Phys.* **6,** 947–950 (2010).

75. Trotta, R. *et al.* Wavelength-tunable sources of entangled photons interfaced with atomic vapours. *Nat. Commun.* **7,** 10375 (2016).
76. Patel, R. B. *et al.* Quantum interference of electrically generated single photons from a quantum dot. *Nanotechnology* **21,** 274011 (2010).
77. Flagg, E. B. *et al.* Interference of single photons from two separate semiconductor quantum dots. *Phys. Rev. Lett.* **104,** 137401 (2010).
78. Moreau, E. *et al.* Quantum cascade of photons in semiconductor quantum dots. *Phys. Rev. Lett.* **87,** 183601 (2001).
79. Santori, C., Solomon, G. S., Pelton, M. & Yamamoto, Y. Time-resolved spectroscopy of multiexcitonic decay in an InAs quantum dot. *Phys. Rev. B* **65,** 073310 (2002).
80. Muller, A., Fang, W., Lawall, J. & Solomon, G. S. Emission spectrum of a dressed exciton–biexciton complex in a semiconductor quantum dot. *Phys. Rev. Lett.* **101,** 027401 (2008).
81. Melet, R. *et al.* Resonant excitonic emission of a single quantum dot in the Rabi regime. *Phys. Rev. B* **78,** 073301 (2008).
82. Jayakumar, H. *et al.* Deterministic photon pairs and coherent optical control of a single quantum dot. *Phys. Rev. Lett.* **110,** 135505 (2013).
83. He, Y.-M. *et al.* On-demand semiconductor single-photon source with near-unity indistinguishability. *Nat. Nanotech.* **8,** 213–217 (2013).
84. Müller, M., Bounouar, S., Jöns, K. D., Glässl, M. & Michler, P. On-demand generation of indistinguishable polarization-entangled photon pairs. *Nat. Photon.* **8,** 224–228 (2014).
85. Yuan, Z. *et al.* Electrically driven single-photon source. *Science* **295,** 102–105 (2002).
86. Flagg, E. B., Polyakov, S. V., Thomay, T. & Solomon, G. S. Dynamics of nonclassical light from a single solid-state quantum emitter. *Phys. Rev. Lett.* **109,** 163601 (2012).
87. Giesz, V. *et al.* Influence of the Purcell effect on the purity of bright single photon sources. *Appl. Phys. Lett.* **103,** 033113 (2013).
88. Wei, Y.-J. *et al.* Deterministic and robust generation of single photons from a single quantum dot with 99.5% indistinguishability using adiabatic rapid passage. *Nano Lett.* **14,** 6515–6519 (2014).
89. Ding, X. *et al.* On-demand single photons with high extraction efficiency and near-unity indistinguishability from a resonantly driven quantum dot in a micropillar. *Phys. Rev. Lett.* **116,** 020401 (2016).
90. Unsleber, S. *et al.* Highly indistinguishable on-demand resonance fluorescence photons from a deterministic quantum dot micropillar device with 74% extraction efficiency. *Opt. Express* **24,** 8539–8546 (2016).
91. Benson, O., Santori, C., Pelton, M. & Yamamoto, Y. Regulated and entangled photons from a single quantum dot. *Phys. Rev. Lett.* **84,** 2513–2516 (2000).
92. Young, R. J. *et al.* Improved fidelity of triggered entangled photons from single quantum dots. *New J. Phys.* **8,** 29–29 (2006).
93. Akopian, N. *et al.* Entangled photon pairs from semiconductor quantum dots. *Phys. Rev. Lett.* **96,** 130501 (2006).
94. Juska, G., Dimastrodonato, V., Mereni, L. O., Gocalinska, A. & Pelucchi, E. Towards quantum-dot arrays of entangled photon emitters. *Nat. Photon.* **7,** 527–531 (2013).
95. Stevenson, R. M. Magnetic-field-induced reduction of the exciton polarisation splitting in InAs quantum dots. *Phys. Rev. B* **73,** 033306 (2006).
96. Zhang, J. *et al.* High yield and ultrafast sources of electrically triggered entangled-photon pairs based on strain-tunable quantum dots. *Nat. Commun.* **6,** 10067 (2015).
97. Muller, A., Fang, W., Lawall, J. & Solomon, G. S. Creating polarization-entangled photon pairs from a semiconductor quantum dot using the optical Stark effect. *Phys. Rev. Lett.* **103,** 217402 (2009).
98. Trotta, R., Wildmann, J. S., Zallo, E., Schmidt, O. G. & Rastelli, A. Highly entangled photons from hybrid piezoelectric-semiconductor quantum dot devices. *Nano Lett.* **14,** 3439–3444 (2014).
99. Kiraz, A., Atature, M. & Imamoglu, A. Quantum-dot single-photon sources: prospects for applications in linear optics quantum-information processing. *Phys. Rev. A* **69,** 032305 (2004).
100. Santori, C., Fattal, D., Vuckovic, J., Solomon, G. S. & Yamamoto, Y. Indistinguishable photons from a single-photon device. *Nature* **419,** 594–597 (2002).
101. Borri, P. *et al.* Ultralong dephasing time in InGaAs quantum dots. *Phys. Rev. Lett.* **87,** 157401 (2001).
102. Kammerer, C. *et al.* Efficient acoustic phonon broadening in single self-assembled InAs/GaAs quantum dots. *Phys. Rev. B* **65,** 033313 (2001).
103. Grange, T. Decoherence in quantum dots due to real and virtual transitions: a nonperturbative calculation. *Phys. Rev. B* **80,** 245310 (2009).
104. Thoma, A. *et al.* exploring dephasing of a solid-state quantum emitter via time- and temperature-dependent Hong–Ou–Mandel experiments. *Phys. Rev. Lett.* **116,** 033601 (2016).
105. Kuhlmann, A. V. *et al.* Charge noise and spin noise in a semiconductor quantum device. *Nat. Phys.* **9,** 570–575 (2013).
106. Berthelot, A. *et al.* Unconventional motional narrowing in the optical spectrum of a semiconductor quantum dot. *Nat. Phys.* **2,** 759–764 (2006).
107. Varoutsis, S. *et al.* Restoration of photon indistinguishability in the emission of a semiconductor quantum dot. *Phys. Rev. B* **72,** 041303 (2005).
108. Grange, T. *et al.* Reducing phonon-induced decoherence in solid-state single-photon sources with cavity quantum electrodynamics. *Phys. Rev. Lett.* **118,** 253602 (2017).
109. Besombes, L., Kheng, K., Marsal, L. & Mariette, H. Acoustic phonon broadening mechanism in single quantum dot emission. *Phys. Rev. B* **63,** 155307 (2001).
110. Favero, I. *et al.* Acoustic phonon sidebands in the emission line of single InAs/GaAs quantum dots. *Phys. Rev. B* **68,** 233301 (2003).
111. Kaer, P. Decoherence in semiconductor cavity QED systems due to phonon couplings. *Phys. Rev. B* **90,** 035312 (2014).
112. Gazzano, O. *et al.* Bright solid-state sources of indistinguishable single photons. *Nat. Commun.* **4,** 1425 (2013).
113. Ates, S. *et al.* Post-selected indistinguishable photons from the resonance fluorescence of a single quantum dot in a microcavity. *Phys. Rev. Lett.* **103,** 167402 (2009).
114. Nguyen, H. S. *et al.* Ultra-coherent single photon source. *Appl. Phys. Lett.* **99,** 261904 (2011).
115. Matthiesen, C., Vamivakas, A. N. & Atatuere, M. Subnatural linewidth single photons from a quantum dot. *Phys. Rev. Lett.* **108,** 093602 (2012).
116. Reimer, M. E. Overcoming power broadening of the quantum dot emission in a pure wurtzite nanowire. *Phys. Rev. B* **93,** 195316 (2016).
117. Kuhlmann, A. V. *et al.* Transform-limited single photons from a single quantum dot. *Nat. Commun.* **6,** 8204 (2015).
118. Loredo, J. C. *et al.* Scalable performance in solid-state single-photon sources. *Optica* **3,** 433–440 (2016).
119. Wang, H. *et al.* Near-transform-limited single photons from an efficient solid-state quantum emitter. *Phys. Rev. Lett.* **116,** 213601 (2016).
120. Pelton, M. *et al.* Efficient source of single photons: a single quantum dot in a micropost microcavity. *Phys. Rev. Lett.* **89,** 233602 (2002).
121. Purcell, E. M., Torrey, H. C. & Pound, R. V. Resonance absorption by nuclear magnetic moments in a solid. *Phys. Rev.* **69,** 37–38 (1946).
122. Gerard, J. M. *et al.* Enhanced spontaneous emission by quantum boxes in a monolithic optical microcavity. *Phys. Rev. Lett.* **81,** 1110–1113 (1998).
123. Yablonovitch, E. Inhibited spontaneous emission in solid-state physics and electronics. *Phys. Rev. Lett.* **58,** 2059–2062 (1987).
124. Haroche, S. & Kleppner, D. Cavity quantum electrodynamics. *Phys. Today* **42,** 24–30 (2008).
125. Solomon, G. S., Pelton, M. & Yamamoto, Y. Single-mode spontaneous emission from a single quantum dot in a three-dimensional microcavity. *Phys. Rev. Lett.* **86,** 3903–3906 (2001).
126. Kiraz, A. *et al.* Cavity-quantum electrodynamics using a single InAs quantum dot in a microdisk structure. *Appl. Phys. Lett.* **78,** 3932–3934 (2001).
127. Englund, D. *et al.* Controlling the spontaneous emission rate of single quantum dots in a two-dimensional photonic crystal. *Phys. Rev. Lett.* **95,** 013904 (2005).
128. Yoshie, T. *et al.* Vacuum Rabi splitting with a single quantum dot in a photonic crystal nanocavity. *Nature* **432,** 200–203 (2004).
129. Reithmaier, J. P. *et al.* Strong coupling in a single quantum dot–semiconductor microcavity system. *Nature* **432,** 197–200 (2004).
130. Peter, E. *et al.* Exciton–photon strong-coupling regime for a single quantum dot embedded in a microcavity. *Phys. Rev. Lett.* **95,** 067401 (2005).
131. Auffèves-Garnier, A., Simon, C., Gérard, J.-M. & Poizat, J.-P. Giant optical nonlinearity induced by a single two-level system interacting with a cavity in the Purcell regime. *Phys. Rev. A* **75,** 053823 (2007).
132. Arnold, C. *et al.* Optical bistability in a quantum dots/micropillar device with a quality factor exceeding 200 000. *Appl. Phys. Lett.* **100,** 111111 (2012).
133. Schneider, C., Gold, P., Reitzenstein, S., Höfling, S. & Kamp, M. Quantum dot micropillar cavities with quality factors exceeding 250,000. *Appl. Phys. B* **122,** 19 (2016).
134. Stoltz, N. G. *et al.* High-quality factor optical microcavities using oxide apertured micropillars. *Appl. Phys. Lett.* **87,** 031105 (2005).
135. Moreau, E. *et al.* Single-mode solid-state single photon source based on isolated quantum dots in pillar microcavities. *Appl. Phys. Lett.* **79,** 2865–2867 (2001).
136. Strauf, S. *et al.* High-frequency single-photon source with polarization control. *Nat. Photon.* **1,** 704–708 (2007).
137. Heindel, T. *et al.* Electrically driven quantum dot–micropillar single photon source with 34% overall efficiency. *Appl. Phys. Lett.* **96,** 011107 (2010).
138. Giesz, V. *et al.* Cavity-enhanced two-photon interference using remote quantum dot sources. *Phys. Rev. B* **92,** 161302 (2015).
139. Lermer, M. *et al.* Bloch-wave engineering of quantum dot micropillars for cavity quantum electrodynamics experiments. *Phys. Rev. Lett.* **108,** 057402 (2012).

140. Laurent, S. *et al.* Indistinguishable single photons from a single-quantum dot in a two-dimensional photonic crystal cavity. *Appl. Phys. Lett.* **87,** 163107 (2005).
141. Madsen, K. H. *et al.* Efficient out-coupling of high-purity single photons from a coherent quantum dot in a photonic-crystal cavity. *Phys. Rev. B* **90,** 155303 (2014).
142. Laucht, A. *et al.* Electrical control of spontaneous emission and strong coupling for a single quantum dot. *New J. Phys.* **11,** 023034 (2009).
143. Bennett, A. J. *et al.* Giant Stark effect in the emission of single semiconductor quantum dots. *Appl. Phys. Lett.* **97,** 031104 (2010).
144. Böckler, C. *et al.* Electrically driven high-*Q* quantum dot–micropillar cavities. *Appl. Phys. Lett.* **92,** 091107 (2008).
145. Nowak, A. K. *et al.* Deterministic and electrically tunable bright single-photon source. *Nat. Commun.* **5,** 3240 (2014).
146. Lund-Hansen, T. *et al.* Experimental realization of highly efficient broadband coupling of single quantum dots to a photonic crystal waveguide. *Phys. Rev. Lett.* **101,** 113903 (2008).
147. Claudon, J. *et al.* A highly efficient single-photon source based on a quantum dot in a photonic nanowire. *Nat. Photon.* **4,** 174–177 (2010).
148. Reimer, M. E. *et al.* Bright single-photon sources in bottom-up tailored nanowires. *Nat. Commun.* **3,** 737 (2012).
149. Laucht, A. *et al.* A waveguide-coupled on-chip single-photon source. *Phys. Rev. X* **2,** 011014 (2012).
150. Bulgarini, G. *et al.* Nanowire waveguides launching single photons in a Gaussian mode for ideal fiber coupling. *Nano Lett.* **14,** 4102–4106 (2014).
151. Arcari, M. *et al.* Near-unity coupling efficiency of a quantum emitter to a photonic crystal waveguide. *Phys. Rev. Lett.* **113,** 093603 (2014).
152. Babinec, T. M. *et al.* A diamond nanowire single-photon source. *Nat. Nanotech.* **5,** 195–199 (2010).
153. Bleuse, J. *et al.* Inhibition, enhancement, and control of spontaneous emission in photonic nanowires. *Phys. Rev. Lett.* **106,** 103601 (2011).
154. Hoang, T. B. *et al.* Enhanced spontaneous emission from quantum dots in short photonic crystal waveguides. *Appl. Phys. Lett.* **100,** 061122 (2012).
155. Munsch, M. *et al.* Dielectric GaAs antenna ensuring an efficient broadband coupling between an InAs quantum dot and a Gaussian optical beam. *Phys. Rev. Lett.* **110,** 177402 (2013).
156. Gazzano, O. *et al.* Single photon source using confined Tamm plasmon modes. *Appl. Phys. Lett.* **100,** 232111 (2012).
157. Kumano, H. *et al.* Enhanced photon extraction from a quantum dot induced by a silver microcolumnar photon reflector. *Appl. Phys. Express* **6,** 062801 (2013).
158. Sapienza, L., Davanço, M., Badolato, A. & Srinivasan, K. Nanoscale optical positioning of single quantum dots for bright and pure single-photon emission. *Nat. Commun.* **6,** 7833 (2015).
159. Gschrey, M. *et al.* *In situ* electron-beam lithography of deterministic single-quantum-dot mesa-structures using low-temperature cathodoluminescence spectroscopy. *Appl. Phys. Lett.* **102,** 251113 (2013).
160. Gschrey, M. *et al.* Highly indistinguishable photons from deterministic quantum-dot microlenses utilizing three-dimensional *in situ* electron-beam lithography. *Nat. Commun.* **6,** 7662 (2015).
161. Portalupi, S. L. *et al.* Bright phonon-tuned single-photon source. *Nano Lett.* **15,** 6290–6294 (2015).
162. Gazzano, O. *et al.* Entangling quantum-logic gate operated with an ultrabright semiconductor single-photon source. *Phys. Rev. Lett.* **110,** 250501 (2013).
163. Wang, H. *et al.* High-efficiency multiphoton boson sampling. *Nat. Photon.* **11,** 361–365 (2017).
164. Takemoto, K. *et al.* Transmission experiment of quantum keys over 50 km using high-performance quantum-dot single-photon source at 1.5 μm wavelength. *Appl. Phys. Express* **3,** 092802 (2010).
165. Schneider, C. *et al.* Microcavity enhanced single photon emission from an electrically driven site-controlled quantum dot. *Appl. Phys. Lett.* **100,** 091108 (2012).
166. Badolato, A. *et al.* Deterministic coupling of single quantum dots to single nanocavity modes. *Science* **308,** 1158–1161 (2005).
167. Hennessy, K. *et al.* Quantum nature of a strongly coupled single quantum dot–cavity system. *Nature* **445,** 896–899 (2007).
168. Dousse, A. *et al.* Controlled light-matter coupling for a single quantum dot embedded in a pillar microcavity using far-field optical lithography. *Phys. Rev. Lett.* **101,** 267404 (2008).
169. Sawicki, K. *et al.* Single-color, *in situ* photolithography marking of individual CdTe/ZnTe quantum dots containing a single Mn^{2+} ion. *Appl. Phys. Lett.* **106,** 012101 (2015).
170. Sartison, M. *et al.* Combining *in-situ* lithography with 3D printed solid immersion lenses for single quantum dot spectroscopy. *Sci. Rep.* **7,** 39916 (2017).
171. Dousse, A. *et al.* Scalable implementation of strongly coupled cavity-quantum dot devices. *Appl. Phys. Lett.* **94,** 121102 (2009).
172. Lee, K. H. *et al.* Registration of single quantum dots using cryogenic laser photolithography. *Appl. Phys. Lett.* **88,** 193106 (2006).
173. Thon, S. M. *et al.* Strong coupling through optical positioning of a quantum dot in a photonic crystal cavity. *Appl. Phys. Lett.* **94,** 111115 (2009).
174. Steinmetz, T. *et al.* Stable fiber-based Fabry-Pérot cavity. *Appl. Phys. Lett.* **89,** 111110 (2006).
175. Muller, A., Flagg, E. B., Metcalfe, M., Lawall, J. & Solomon, G. S. Coupling an epitaxial quantum dot to a fiber-based external-mirror microcavity. *Appl. Phys. Lett.* **95,** 173101 (2009).
176. Miguel-Sánchez, J. *et al.* Cavity quantum electrodynamics with charge-controlled quantum dots coupled to a fiber Fabry–Perot cavity. *New J. Phys.* **15,** 045002 (2013).
177. Greuter, L. *et al.* A small mode volume tunable microcavity: development and characterization. *Appl. Phys. Lett.* **105,** 121105 (2014).
178. Göbel, E. O. & Siegner, U. in *Quantum Metrology: Foundation of Units and Measurements* 191–206 (Wiley-VCH, 2015).
179. White, A. G., Mitchell, J. R., Nairz, O. & Kwiat, P. G. "Interaction-free" imaging. *Phys. Rev. A* **58,** 605–613 (1998).
180. Loredo, J. C. *et al.* Boson sampling with single-photon Fock states from a bright solid-state source. *Phys. Rev. Lett.* **118,** 130503 (2017).
181. Patel, R. B. *et al.* Two-photon interference of the emission from electrically tunable remote quantum dots. *Nat. Photon.* **4,** 632–635 (2010).
182. Gao, W. B. *et al.* Quantum teleportation from a propagating photon to a solid-state spin qubit. *Nat. Commun.* **4,** 2744 (2013).
183. Akopian, N., Wang, L., Rastelli, A., Schmidt, O. G. & Zwiller, V. Hybrid semiconductor-atomic interface: slowing down single photons from a quantum dot. *Nat. Photon.* **5,** 230–233 (2011).
184. Kim, J.-H., Cai, T., Richardson, C. J. K., Leavitt, R. P. & Waks, E. Two-photon interference from a bright single-photon source at telecom wavelengths. *Optica* **3,** 577–584 (2016).
185. Takemoto, K. *et al.* Quantum key distribution over 120 km using ultrahigh purity single-photon source and superconducting single-photon detectors. *Sci. Rep.* **5,** 14383 (2015).
186. Zaske, S. *et al.* Visible-to-telecom quantum frequency conversion of light from a single quantum emitter. *Phys. Rev. Lett.* **109,** 147404 (2012).
187. Ates, S. *et al.* Two-photon interference using background-free quantum frequency conversion of single photons emitted by an InAs quantum dot. *Phys. Rev. Lett.* **109,** 147405 (2012).
188. Pelc, J. S. *et al.* Downconversion quantum interface for a single quantum dot spin and 1550-nm single-photon channel. *Opt. Express* **20,** 27510 (2012).
189. Brown, R. H. & Twiss, R. Q. Correlation between photons in two coherent beams of light. *Nature* **177,** 27–29 (1956).
190. Stevens, M. in *Single-Photon Generation and Detection* (eds Migdall, A. *et al.*) Vol. 45 25–68 (Academic Press, 2013).

Acknowledgements

P.S. acknowledges partial support from the ERC Starting Grant No. 277885 QD-CQED. A.W. acknowledges partial support from the Australian Research Centres of Excellence for Engineered Quantum Systems (CE110001013) and Quantum Computing and Communication Technology (CE110001027). G.S. acknowledges partial support from the PFC@JQI.

Additional information

Reprints and permissions information is available online at www.nature.com/reprints. Publisher's note: Springer Nature remains neutral with regard to jurisdictional claims in published maps and institutional affiliations. Correspondence and requests for materials should be addressed to P.S.

Competing financial interests

P.S. is co-founder and scientific advisor of the single-photon-source company Quandela.